Structural basis for polyproline-mediated ribosome stalling and rescue by the translation elongation factor EF-P

Paul Huter[1], Stefan Arenz[1], Lars V. Bock[2], Michael Graf[1], Jan Ole Frister[3], Andre Heuer[1], Lauri Peil[4], Agata L. Starosta[1,§], Ingo Wohlgemuth[3], Frank Peske[3], Jirka Novacek[5], Otto Berninghausen[1], Helmut Grubmüller[2], Tanel Tenson[4], Roland Beckmann[1], Marina V. Rodnina[3], Andrea C. Vaiana[2], Daniel N. Wilson[1,6*]

[1] Gene Center, Department for Biochemistry and Center for integrated Protein Science Munich (CiPSM), University of Munich, Feodor-Lynenstr. 25, 81377 Munich, Germany
[2] Department of Theoretical and Computational Biophysics, Max Planck Institute for Biophysical Chemistry, Am Fassberg 11, Göttingen 37077, Germany.
[3] Department of Physical Biochemistry, Max Planck Institute for Biophysical Chemistry, Am Fassberg 11, 37077 Göttingen, Germany.
[4] University of Tartu, Institute of Technology, Nooruse 1, 50411 Tartu, Estonia
[5] Central European Institute of Technology (CEITEC), Masaryk University, Kamenice 5, 62500 Brno, Czech Republic.
[6] Institute for Biochemistry and Molecular Biology, University of Hamburg, Martin-Luther-King-Platz 6, 20146 Hamburg, Germany

*Correspondence: Tel: +49(0)40-42838-2841; Fax: +49(0)40-42838-2848; Email: daniel.wilson@chemie.uni-hamburg.de

§ Present address: Centre for Bacterial Cell Biology, Institute for Cell and Molecular Biosciences, University of Newcastle, Newcastle upon Tyne, United Kingdom.

Running title: Structures of polyproline-stalled ribosomes with EF-P

ABSTRACT (max 140 words)

Ribosomes synthesizing proteins containing consecutive proline residues become stalled and require rescue via the action of uniquely modified translation elongation factors, EF-P in bacteria or archaeal/eukaryotic a/eIF5A. To date no structures exist of EF-P or eIF5A in complex with translating ribosomes stalled at a polyproline stretch and thus structural insight into how EF-P/eIF5A rescue these arrested ribosomes has been lacking. Here we present cryo-EM structures of ribosomes stalled on proline stretches, without and with modified EF-P. The structures suggest that the favored conformation of the polyproline-containing nascent chain is incompatible with the peptide exit tunnel of the ribosome and leads to destabilization of the peptidyl-tRNA. Binding of EF-P stabilizes the P-site tRNA, particularly via interactions between its modification and the CCA-end, thereby enforcing an alternative conformation of the polyproline-containing nascent chain, which promotes a favorable geometry for peptide bond formation.

Ribosomes catalyze the synthesis of proteins in cells by providing a platform for the binding of tRNAs. There are three tRNA binding sites on the ribosome, the A-, P- and E-sites. During translation elongation, aminoacyl-tRNAs (aa-tRNAs) binding at the A-site undergo peptide bond formation with the peptidyl-tRNA located at the P-site. The rate of peptide bond formation is influenced by the chemical nature of the amino acid substrates in both the A- and P-sites. Among other amino acids, proline is a particularly poor substrate both as donor and acceptor during peptide bond formation[1-6]. In fact, ribosomes become stalled when ribosomes synthesize proteins containing consecutive proline residues[5,7,8]. To alleviate the ribosome stalling and allow translation to continue, a specialized translation factor is required, elongation factor P (EF-P) in bacteria or initiation factor 5A (IF5A) in archaea and eukaryotes[5,7,9]. IF5A has been shown to be essential in eukaryotes[10] and deletion of *efp* in some bacteria leads to growth defects and avirulence[11].

Both EF-P and IF5A bear post-translational modifications that are essential for their rescue activity[5,7,9,12]. In *Escherichia coli*, lysine 34 (K34) of EF-P is post-translationally modified by the combined action of EpmA (YjeA), EpmB (YjeK) and EpmC (YfcM). EpmB converts (S)-α-lysine to (R)-β-lysine[13] and EpmA ligates the (R)-β-lysine to the ε-amino group of K34[14,15]. EpmC recognizes the modified form of EF-P and hydroxylates the C5(δ) of K34[16], however, the hydroxylation is not required for the rescue activity of EF-P[5,7]. Surprisingly, the resulting ε(R)-β-lysylhydroxylysine modification of *E. coli* EF-P and the enzymes associated with this modification are not conserved across all bacteria[17,18]. Instead, unrelated enzymes and/or modifications have been identified in other bacteria. In *Pseudomonas aeruginosa* and *Shewanella oneidensis* EarP catalyzes the addition of rhamnose to arginine 32 (R32) of EF-P[18,19], whereas *Bacillus subtilis* is reported to bear an 5-aminopentanol moiety attached to K32[20]. In eukaryotes, a conserved lysine residue is post-translationally modified to hypusine by the action of deoxyhypusine synthase (DHS) and deoxyhypusine hydroxylase (DOHH)[10,11].

The structure of bacterial EF-P revealed a three-domain architecture, with the modified residue located at the tip of domain 1[21]. aIF5A and eIF5A are homologous to bacterial EF-P domains 1 and 2, but lack the bacterial-specific domain 3[10,11]. The X-ray structure of unmodified *Thermus thermophilus* EF-P in complex with *T. thermophilus*

70S ribosome bearing a deacylated $tRNA^{fMet}$ at the P-site revealed that EF-P binds within the E-site of the ribosome with the unmodified arginine 32 (R32) of EF-P interacting with the CCA-end of the P-site tRNA[22]. Similarly, structures of modified eIF5A on the yeast ribosome also visualized the hypusine modification extending into the peptidyltransferase center (PTC) of the ribosome[23,24] where it interacts with the CCA-end of the P-site tRNA[24]. However, to date no structures exist of EF-P or eIF5A in complex with polyproline-stalled ribosomes, therefore, it remains unclear how the proline residues stall translation and how EF-P/IF5A alleviates these stalled ribosomes.

RESULTS

Structure of a polyproline-stalled ribosome complex

To investigate how polyproline stretches cause translational arrest, we employed a previously used reporter mRNA coding for NlpD-PPP protein bearing three consecutive proline ($_{71}PPP_{73}$) residues[25] (**Fig. 1a**), which was translated in an *E. coli* lysate based S30 translation system derived from an *E. coli efp* deletion strain (see **Methods**). As expected[25], ribosomes with peptidyl-tRNA stalled at the PPP stretch could be alleviated by the exogenous addition of purified modified EF-P protein (**Fig. 1a**). Previous biochemical studies[5,7,8], as well as toeprinting assays using the same NlpD-PPP template[25], indicate that ribosomes stall in the absence of EF-P because of slow peptide bond formation between the peptidyl-Pro-Pro-tRNA in the P-site and the incoming Pro-tRNA in the A-site (**Fig. 1b**). These PPP-stalled ribosomes were purified using the 6 x Histidine-tag located at the N-terminus of the nascent peptide (**Fig. 1b**) and subjected to cryo-EM analysis (**see Methods**). *In silico* sorting of the cryo-EM images yielded two subpopulations of non-rotated ribosomes bearing a P-site tRNA, but differing by the absence or presence of A-site tRNA (17% and 44%, respectively; **Supplementary Fig. 1a**). The cryo-EM structures were refined to yield average resolutions of 3.6 Å and 3.9 Å, respectively (**Fig. 1c,d, Table 1** and **Supplementary Fig. 1b-e**). In addition, a large population (30%) of vacant ribosomes was observed as well as a small population (9%) of 70S ribosomes in a rotated state with hybrid A/P-site and P/E-site tRNAs (**Supplementary Fig. 1a**), the latter presumably representing a post-peptide bond formation state.

The density quality and resolution for the A-site and P-site tRNAs was generally poorer and less uniform than observed in previous ribosomal complexes[26-28]. In particular, the density was well resolved for the anticodon stem loop (ASL) of the tRNA on the 30S subunit and progressively deteriorated towards the elbow and acceptor arm of the tRNAs on the 50S subunit (**Fig. 1e,f** and **Supplementary Fig. 2a-g**). In fact, density for the CCA-end of the P- and A-site tRNAs at the PTC was only present at low thresholds (**Fig. 1g, h**). Local resolution calculations also confirmed the flexible nature of the CCA-end, particularly with respect to the terminal A76 nucleotide (**Supplementary Fig. 2h-j**). In the structure containing only P-site tRNA, no significant density was observed for the nascent polypeptide chain (**Fig. 1g**), whereas in the structure with both A- and P-site tRNAs, the density attributable to the nascent chain was fragmented and disconnected from the tRNAs (**Fig. 1h**). The density for the CCA-end of the A-site tRNA was worse than the P-site tRNA (**Fig. 1d** and **Supplementary Fig. 2d-g**), suggesting that the Pro-tRNA had severe problems to accommodate at the A-site of the PTC. Consistent with this notion, the N-terminus of ribosomal protein L27, which becomes stabilized upon A-site tRNA accommodation[29,30], remained disordered (**Supplementary Fig. 2k**).

The destabilization of the peptidyl-tRNA observed within the structures of the PPP-stalled ribosomes is compatible with the observed peptidyl-tRNA drop-off that was reported to occur when ribosomes stall during translation of short polyproline-containing peptides[5,6]. Indeed, peptidyl-tRNA destabilization, coupled with peptide release and/or ribosome rescue within the translation extracts, may explain the unusually high proportion (30%) of vacant 70S ribosomes that were present in the PPP-stalled ribosome sample following purification (**Supplementary Fig. 1a**). Collectively, our findings suggest that the presence of the polyproline stretch within the nascent polypeptide chain leads to destabilization of the peptidyl-tRNA and prevents accommodation of the aa-tRNA at the A-site, thereby causing translational stalling.

EF-P in complex with PPP-stalled ribosomes

To investigate structurally how EF-P relieves the translation arrest caused by polyproline stretches, PPP-stalled ribosomes were incubated with fully-modified *E. coli* EF-P (**Fig. 2a**) and the resulting complexes were analyzed by cryo-EM. *In silico* sorting of the cryo-

EM data yielded two major subpopulations of ribosomes bearing P-tRNA, distinguished by the presence (30%) or absence of EF-P (33%) (**Supplementary Fig. 1f**). The EF-P-containing subpopulation was extremely heterogeneous and only a stable subpopulation containing A- and P-site tRNAs with EF-P bound in the E-site (**Fig. 2b**) could be refined further, yielding an average resolution of 3.7 Å (**Table 1** and **Supplementary Fig. 1g,h**). Despite multiple attempts, we were unable to obtain a clean subpopulation containing P-site tRNA and EF-P, but lacking A-site tRNA. For completeness, we also refined the major P-site tRNA subpopulation lacking EF-P (**Fig. 2c**) to an average resolution of 3.2 Å (**Table 1** and **Supplementary Fig. 1i,j**). As before (**Fig. 1g**), little density was observed for the nascent polypeptide chain attached to the P-site tRNA in the EF-P lacking structure (**Fig. 2d**), despite the improved quality of the density for the CCA-end of the P-site tRNA. By contrast, additional nascent chain density was observed when EF-P was present (**Fig. 2e**), however, this density fused directly to the A-site tRNA, rather than the P-site tRNA (**Fig. 2f**). Therefore, we concluded that the EF-P-containing subpopulation represents a post-peptide bond formation state with deacylated tRNA in the P-site and peptidyl-tRNA in the A-site. We also observe that the N-terminus of L27 was ordered (**Fig. 2g**), which as mentioned is diagnostic for accommodation of the aa-tRNA at the A-site[29,30].

EF-P in complex with PP-stalled ribosomes without the A-tRNA

In order to capture EF-P bound to polyproline-stalled ribosomes in a pre-peptide bond formation state, we employed a modified version of the NlpD-PPP mRNA that was truncated directly after the codon for the second proline of the PPP motif (**Fig. 3a**). Ribosomes translating the truncated NlpD-PP mRNA become stalled after the PP-motif because the absence of an A-site codon precludes binding of the next aa-tRNA, thus the ribosomes cannot catalyze peptide bond formation even when EF-P is present (**Fig. 3a**). The purified truncated NlpD-PP-stalled ribosomes were then incubated with active modified *E. coli* EF-P (**Fig. 3a**) and the resulting complexes were analyzed by cryo-EM. *In silico* sorting of the cryo-EM data yielded two major subpopulations of ribosomes bearing either P- and E-site tRNAs (22%) or P-site tRNA with EF-P bound in the E-site (74%) (**Supplementary Fig. 1k**). The EF-P containing subpopulation could be further

segregated into ribosome populations that differed with respect to the L1 stalk adopting an "in" (30%) or "out" (44%) conformation. The "in" position of the L1 stalk significantly improved the quality of the EF-P density and therefore this population was further refined, yielding a final cryo-EM structure (**Fig. 3b**) with an average resolution of 3.1 Å (**Table 1** and **Supplementary Fig. 1l,m**). Similarly, we could also refine the major P- and E-site tRNA containing ribosome subpopulation that lacked EF-P (**Fig. 3c**) to a final average resolution of 3.2 Å (**Supplementary Fig. 1n,o**). Local resolution calculations indicate less flexibility of the P-site tRNA in the presence of EF-P (**Fig. 3d**) when compared to ribosomes bound with E-site tRNA (**Fig. 3e**) or having a vacant E-site (**Fig. 3f**), thus supporting the hypothesis that EF-P stabilizes the P-site peptidyl-tRNA on the ribosome.

EF-P residues critical for P-site tRNA interaction

The well-resolved density for *E. coli* EF-P bound to the ribosome population with the L1-"in" conformation enabled a complete molecular model to be generated (**Fig. 4a** and **Supplementary Fig. 3a**). The overall conformation of *E. coli* EF-P on a polyproline-stalled ribosome is very similar to that observed by X-ray crystallography for *T. thermophilus* EF-P bound to a *T. thermophilus* 70S ribosome with a deacylated-$tRNA^{fMet}$ in the P-site[22], whereas it deviates more significantly from the binding position observed for the yeast homologue eIF5A bound to the 80S ribosome[23,24] (**Supplementary Fig. 3b-c**). We observe that the backbone of Asp69 of *E. coli* EF-P is within hydrogen bonding distance of U17a within the D-loop of the peptidyl-$tRNA^{Pro}$ in the P-site (**Supplementary Fig. 3d**). This interaction is also observed in the *T. thermophilus* EF-P-ribosome structure[22] (**Supplementary Fig. 3e**), but is not possible for tRNAs containing shorter D-loops (**Supplementary Fig. 3f**), thus providing a specificity determinant for EF-P to recognize $tRNA^{fMet}$ and $tRNA^{Pro}$ [Ref. [31]] (**Supplementary Fig. 3d,e**). By contrast, such a specific interaction between yeast eIF5A and the P-site tRNA was not observed[23,24], consistent with the diverse range of non-proline containing stalling motifs that are recognized and rescued by eIF5A[32,33].

Unlike eIF5A, bacterial EF-P has an additional domain 3 that contacts the small ribosomal subunit and the ASL of the P-site tRNA (**Fig. 4b**). In particular, two conserved

residues Tyr183 and Arg186 are within hydrogen bonding distance of A42 of the P-site tRNA and G1338 within helix h29 of the 16S rRNA[22] (**Fig. 4b**). To investigate the importance of these interactions, we generated modified EF-P variants bearing Y183A or R186A substitutions, and monitored their ability to promote translation of a polyproline-containing firefly luciferase (Fluc) reporter protein[7] (**Fig. 4c**). In the absence of EF-P, ribosomes stall at the polyproline motif and little or no luminescence is observed because translation of full-length Fluc is prevented. As expected, addition of modified active EF-P rescues the polyproline-stalled ribosomes, leading to production of full-length Fluc and a corresponding increase in luminescence (**Fig. 4c**). By contrast, the EF-P-Y183A and EF-P-R186A variants were both completely inactive, as was the previously reported inactive EF-P-K34A variant[5,7]. These findings demonstrate that the Tyr183 and Arg186 residues are critical for the rescue activity of EF-P and explain their high conservation among bacterial EF-P proteins.

Interaction of EF-P with the mRNA codon in the E site.

In the X-ray structure of *T. thermophilus* EF-P-ribosome structure, loop I of domain 3 of EF-P is disordered[22] (**Fig. 4d**). By contrast, loop I is well-resolved in the cryo-EM structure of *E. coli* EF-P in complex with the PP-stalled ribosome (**Fig. 4a** and **Supplementary Fig. 4a, b**) where it interacts with the ribosomal protein S7 and E-site codon of the mRNA (**Fig. 4d, e**). Binding of EF-P to the ribosome leads to a shift in conformation of the β-hairpin of S7 by 7.4 Å (**Fig. 4d**), which is stabilized via potential hydrogen bond interactions between the sidechain of Arg78 of S7 with the backbone of Gly144 and the sidechain of T146 of EF-P (**Fig. 4d**). Additional interactions are formed between Thr83 and Ser82 of S7 with the backbone of Leu142 and the Asp139 sidechain of EF-P (**Fig. 4e** and **Supplementary Fig. 4c,d**). Loop I of domain 3 of EF-P contains a highly conserved Gly144-Asp145-Thr146 (GDT) motif, which establishes contact with the nucleobase of the first and second positions of the E-site codon of the mRNA (**Fig. 4d,e** and **Supplementary Fig. 4e,f**). To assess the importance of the GDT motif for EF-P activity, we generated modified EF-P bearing a triple substitution of GDT to AAA (EF-P-$_{144}$AAA$_{146}$). Since most of the interactions involve the backbone of the GDT motif, we also generated EF-P variants where 1, 2 or 4 residues within loop I were deleted (EF-P-

loopIΔ1, -loopIΔ2 and -loopIΔ4, respectively). The activity of the EF-P variants was assessed by monitoring the formation of fMPPPF peptide on the ribosome, as described previously[5,6]. As seen in **Figure 4f**, no fMPPPF peptide was synthesized when EF-P was absent, or when the inactive EF-P-K34A variant was used, whereas the presence of wildtype EF-P led to efficient fMPPPF peptide formation. While the EF-P-loopIΔ1 retained wildtype-like activity, the EF-P-$_{144}$AAA$_{146}$ and EF-P-loopIΔ2 variants displayed reduced activity, and the EF-P-loopIΔ4 variant was completely inactive (**Fig. 4f**). Furthermore, an EF-P variant with the complete domain 3 deleted (EF-P-ΔDomain 3) was also inactive (**Fig. 4f**).

These results suggest that the conserved loop I of domain 3 of EF-P is critical for the rescue activity of EF-P and raises the possibility that EF-P recognizes the nature of the E-site codon, analogous to stop codon recognition by the SPF and PXT containing loops of termination RF2 and RF1, respectively[34]. Modeling on the basis of our structure suggests that purines in the first and second position, such as AAA or GGG codons, in the E-site leads to clashes with EF-P, whereas UUU could be accommodated but in a less stable manner (**Supplementary Fig. 5a-d**). In the X-ray structure of *T. thermophilus* EF-P-ribosome structure, the E-site codon was AAA[22] (**Supplementary Fig. 5e,f**), possibly explaining why loop I of domain 3 of EF-P was disordered. Moreover, the -3 nucleotide was also not visualized, supporting the suggestion that EF-P is critical for positioning and stabilization of the E-site codon (**Supplementary Fig. 5e,f**). Further biochemical experiments will be necessary to assess whether loop I of EF-P can really distinguish CCN proline codons in the E-site from other sense codons, and to what extent. The absence of domain 3 in eIF5A does however preclude recognition of the nature of the E-site codon, which may contribute to the relaxed specificity of eIF5A, allowing eIF5A to also act on a diverse range of non-proline containing stalling motifs[32,33].

Stabilization of the CCA-end of the P-tRNA by the EF-P modification

Clear electron density is observed at the tip of domain 1 of EF-P that corresponds to the ε(R)-β-lysylhydroxylysine located at position K34 of EF-P (**Fig. 5a,b**). The post-translation modification extends into a crevice located adjacent to the CCA-end of the P-site tRNA (**Fig. 5a,b**), similar but distinct from that observed previously for the

unmodified R32 residues of *T. thermophilus* EF-P[22], and the hypusine modification located at position K51 of yeast eIF5A[23,24] (**Supplementary Fig. 3g-i**). The structure reveals how the EF-P modification can stabilize the P-site tRNA (**Fig. 5c**) via forming interactions with the backbone of the CCA-end (**Fig. 5b**). Specifically, hydrogen bonds are possible between the ε-amino group of the (R)-lysyl moiety of EF-P and the 2' OH of the ribose of C75 and the bridging oxygen of A76 (**Fig. 5b**). Furthermore, the hydroxyl group that is post-translationally added to K34 of EF-P by EpmC[16] comes within hydrogen binding distance of the 2' OH of C74, but this interaction is unlikely to be critical since EF-P lacking the hydroxylation retains rescue activity[5,7,12]. In addition, the EF-P modification can form hydrogen bonds with the conserved nucleotide A2439 of the 23S rRNA (**Fig. 5b**), analogous to those formed between eIF5A and A2808[23,24], the equivalent residue in the yeast 28S rRNA (**Supplementary Fig. 3i**). By contrast, the overall position and interactions of the modified K34 residue of *E. coli* EF-P differs dramatically from that of the unmodified R32 residues of *T. thermophilus* EF-P[22], which is significantly shorter and interacts only with the nucleobase of C75 of the P-site tRNA (**Supplementary Fig. 3h**).

The conformation of the nascent chain in the presence of EF-P

The presence of additional density for the nascent polypeptide chain attached to the P-tRNA (**Fig. 5c,d**) suggests that by stabilizing the P-site tRNA, EF-P also indirectly stabilizes the nascent chain. Nevertheless, local resolution calculations indicate that the nascent chain is still relatively flexible (**Fig. 5c**), permitting only the four C-terminal residues to be tentatively modeled into the density (**Fig. 5d**). To compare the C-terminal Pro-Pro residues in our structure to other known conformations of Pro-Pro peptides, we initially aligned the X-ray structure of a short CCA-Pro-Pro tRNA mimic bound to the yeast 80S ribosome[35] (**Fig. 5e**). These two proline residues adopt an *all-trans* conformation, which is present in type II polyproline helices (**Fig. 5f**), and also observed in other diprolyl-containing proteins, such as ribosomal proteins S11 and L11[36], and the ribosome-bound antimicrobial peptide Onc112[37,38] (**Supplementary Fig. 6a-c**). However, this conformation cannot occur on the ribosome because it would produce a steric clash between the -2 residue of the nascent chain and nucleotide G2061 of the 23S rRNA that

comprises part of the ribosomal exit tunnel (**Fig. 5f** and **Supplementary Fig. 6a-c**). Similarly, an *all-cis* conformation of the two prolyl residues is also not compatible with the density, nor with translation, since it directs the nascent chain into the ribosomal A-site (**Fig. 5g**). Instead, the diprolyl moiety appears to adopt an alternative *trans* conformation, allowing the -2 residue of the nascent chain to bypass G2061 and extend into the lumen of the ribosomal tunnel (**Fig. 5d**). Although higher resolution will be required to accurately describe the trans conformation in detail, our model suggests that the backbone Psi angle of ~120° is identical with the all-*trans* conformation, but the Phi angle of approximately -90° differs by ~30° from the all-trans Phi angle (-60°). This alternative conformation appears to be similar to that observed on the ribosome for the diprolyl-containing CMV-stalling peptidyl-tRNA[39] (**Supplementary Fig. 6d**), and the overall path of the nascent chain is similar to that observed for other stalling nascent polypeptide chains observed on the ribosome, such as TnaC[40], VemP[41], MifM[42], SecM[43] (**Supplementary Fig. 6e,f**). We suggest the incompatibility between the preferred diprolyl conformation of the nascent chain and the ribosome induces a strained conformation that can be is relieved either by (i) destabilization of the P-site peptidyl-tRNA and therefore ribosomal stalling ensues, or (ii) binding of EF-P that stabilizes the P-site peptidyl-tRNA and forces the nascent chain to adopt an alternative conformation, with the outcome that peptide bond formation can occur.

EF-P stabilizes the P-site tRNA in a pre-attack conformation

To assess the dynamics of the region surrounding the PTC in the presence of modified EF-P, unmodified EF-P or absence of EF-P, we carried out all-atom explicit-solvent molecular dynamics (MD) simulations. The first MD simulation was initiated using the model of the cryo-EM structure of the NlpD-PP-EF-P-ribosome, and two subsequent simulations were performed where either the β-lysine part of modification on K34 or the entire EF-P protein were computationally removed. A total of 15 simulations, 2 μs each, accumulating to a total simulation run time of 30 μs were performed using a reduced system encompassing a 35 Å radius from the PTC. Principal Component Analysis (PCA)[44] was used to extract the two most dominant conformational modes of motion. As shown in **Figure 6a**, in the presence of modified EF-P, the major conformations are

stable and remain close to the cryo-EM structure, which is similar to that observed in the X-ray structures of the *T. thermophilus* pre-attack conformation[29] as well as uninduced and induced conformations from *H. marismortui*[45]. By contrast, after the β -lysine modification of EF-P or the complete EF-P protein was removed from the simulation, the system explored new conformations, moving away from the conformations observed in presence of EF-P, particularly with respect to conformational mode 2 (**Fig. 6, c**). Since conformational mode 2 reflects the relative distance between the α-amino group of an aminoacyl-tRNA in the A-site and the carbonyl-carbon of the aminoacyl ester linkage in the peptidyl-Pro-Pro-tRNA (**Supplementary Fig. 7**), the MD simulations suggest that when the EF-P modification or the entire EF-P protein was absent, the peptidyl-tRNA moved away from the A-site tRNA, generating a geometry that is incompatible with peptide bond formation (**Fig. 6d, e**). By contrast, the presence of the EF-P modification stabilized the pre-attack conformation of the P-site tRNA, thus promoting peptide bond formation (**Fig. 6d**).

CONCLUSION

Collectively, our biochemical and structural findings, together with the available literature, lead us to propose a model for polyproline-mediated translational stalling and rescue by EF-P (**Fig. 7**). Ribosomes translating proteins containing polyproline-stretches become stalled because of slow peptide bond formation between the peptidyl-Pro-Pro-tRNA in the P-site and the incoming Pro-tRNA in the A-site[5] (**Fig. 7a**). The favourable *all-trans* conformation of the Pro-Pro peptide is not possible within the context of the ribosomal tunnel, which leads to destabilization of the P-site tRNA and nascent chain (**Fig. 7b**). For short oligo-peptidyl-tRNAs, this results in high levels of peptidyl-tRNA drop-off[5]. For longer peptidyl-tRNAs that are more refractory to drop-off, the destabilized peptidyl-tRNA results in suboptimal positioning for peptide-bond formation and may also disfavour accommodation of the aminoacyl-tRNA at the A-site (**Fig. 7b**). Polyproline-stalled ribosomes are recognized by EF-P, which utilizes features of the E-site codon of the mRNA as well as specific interactions with D-loop of the P-site Pro-tRNA[31], the L1 stalk and the 30S subunit to promote binding[22] (**Fig. 7c**). While the presence of EF-P generally stabilizes the binding of the P-site tRNA, the ε(R)-β-

lysylhydroxylysine is necessary to specifically interact and stabilize the CCA-end at the PTC (**Fig. 7d**). Stabilization of the CCA-end by the ε(R)-β-lysylhydroxylysine modification of EF-P also positions the nascent polypeptide chain such that it extends into the lumen of the tunnel (**Fig. 7e**), thus allowing the CCA-ends of the tRNAs to adopted the conformation that favors peptide bond formation (**Fig. 7f**). It will be interesting to see how the distinct modifications found on EF-P in other bacteria, such as the rhamnosylation found in *P. aeurignosa* EF-P[18,19] or the 5-aminopentanol moiety of *B. subtilis* EF-P[20], stabilize the CCA-end of the P-site tRNA to promote an optimal geometry for peptide-bond formation. Moreover, although it remains to be determined as to what promotes EF-P dissociation from the ribosome following peptide bond formation, our structure suggests that subunit rotation and opening of the L1 stalk are good candidates for destabilization of EF-P binding.

METHODS (Methods typically do not exceed 3,000 words.)

Preparation of the *E. coli* Δ*efp* S12 translation extract

The *E. coli* Δ*efp* S12 translation extract was prepared as described for *B. subtilis* S12 translation extract[42] with some minor modifications. *E. coli* Δ*efp* cells (Keio collection BW25113) were grown to OD_{600}=5.8 in an 'INFORCE HT minifors' bench-top fermenter in 2xYPTG (16 g/l peptone, 10 g/l yeast extract, 5 g/l NaCl, 22 mM NaH_2PO_4, 40 mM Na_2HPO_4, 19.8 g/l glucose) at 37°C while maintaining pH 7.0 and oxygen level (60%). Cells were collected at 5,000 x *g* at 4°C for 15 min. 22 g of cells were resuspended in 14.6 ml of Buffer A (10 mM Tris-acetate, pH 8.2, 14 mM magnesium acetate, 60 mM potassium glutamate, 1 mM dithiothreitol and 6 mM 2-mercaptoethanol) and broken open in an 'microfluidics model 110I lab homogenizer', 3x at 15,000 psi. Subsequently, the lysate was cleared at 12,000 x *g* and incubated for 30 min at 37°C in a water bath. The cell extract was aliquoted, snap frozen and stored at -80°C.

PCR and *in vitro* transcription

Full-length *nlpD-PPP* construct with a N-terminal 6 x Histidine-tag was amplified from pET-21b-$_{R1}$nlpD[25] using T7 forward (5'-TAATACGACTCACTATAGGG-3') and T7 terminator (5'GCTAGTTATTGCTCAGCGG-3') primer. Truncated *nlpD-PP* construct was amplified from *nlpD-PPP* PCR product using T7 forward and revPP (5'-CGGCGGTCTAATCAACATAC-3') primer. To avoid contamination with remaining full-length *nlpD-PPP* product, *nlpD-PP* was excised from the agarose gel and a second PCR was performed using the excised product as a template with T7 forwards and revPP as primers. PCR products were purified and *in vitro* transcription reaction was performed using 2 µg of PCR product per 100 µl reaction volume and T7 RNA polymerase[42]. The RNA was purified by LiCl/ethanol precipitation.

Preparation of full-length NlpD-PPP-SRC and truncated NlpD-PP-SRC

Full-length NlpD-PPP-SRC was prepared using *E. coli* Δ*efp* S12 translation extract following the procedure described for the *B. subtilis* MifM-SRC[42], except that the volume was 2011 µl for the reaction mix and 489 µl of mRNA were added. *In vitro* translation was carried out for 20 min. Translation reaction was stopped by adding ice cold Buffer B

(50 mM HEPES pH 7.2 at 4°C, 250 mM KOAc, 10 mM MgOAc, 0,1% DDM, 1/1,000 complete protease inhibitor (Roche), 0.2 U/ml RNasin). For the truncated NlpD-PP-SRC, the *in vitro* reaction was carried out using PURExpress *In Vitro* Protein Synthesis Kit (NEB #6800). The translation reaction (750 µl in total) was prepared according to the protocol of the PURExpress *In Vitro Protein* Synthesis Kit but was supplemented with 5 µM anti-ssrA oligo (5'TTAAGCTGCTAAAGCGTAGTTTTCGTCGTTTGCGACTA-3'). Translation was started by adding the truncated *nlpD-PP* PCR product and then the reaction was incubated at 37°C for 20 min with shaking at 1,000 rpm. The SRCs were then purified according to Sohmen et al (2015)[42] with some minor modification. The SRCs on the Talon metal affinity chromatography column were washed with Buffer B for NlpD-PPP-SRC (Dataset 1) or Buffer C (same as Buffer B but with 500 mM KOAc instead of 250 mM KOAc), for Dataset 2 and 3.

Generation and purification of modified EF-P and mutants

Modified active EF-P was purified as described[16]. All EF-P variants were generated by site-directed mutagenesis PCR, similarly as described for TetM variants by Arenz et al (2015)[46]. The EF-P variants were overexpressed in *E. coli* BL21 cells grown at 37°C from overnight culture in lysogeny broth (LB) medium and in the presence of 100 µg/mL ampicillin. Protein expression was induced at an OD_{600} of 0.4 with a final concentration of 1 mM isopropyl-β-D-1-thiogalactopyranoside (IPTG) (Roth). Proteins were expressed from pET-plasmids (listed in **Supplementary Table 1**). To ensure post-translational modification, the EF-P variants were co-expressed with YjeA and YjeK from pRSFDuet vector. After 1 hour of expression cells were lysed using a microfluidizer. The cell lysate was cleared using a SS34 rotor at 4°C and 44,100 x g for 30 minutes. Purification of His-tagged proteins was done with Protino Ni-NTA agarose beads (Macherey-Nagel). The final eluate was applied onto a Superdex HiLoad S75 16/600 column (GE Healthcare) to yield the final concentrated protein in gel filtration buffer (50 mM HEPES pH 7.4, 50 mM KCl, 100 mM NaCl and 5 mM 2-mercaptoethanol).

Luminescence determination of firefly luciferase

In vitro translation of the firefly luciferase was performed using the PURExpress *in vitro* translation kit. For template generation Fluc3xPro was amplified via PCR using T7 forward and T7 reverse primer (**Supplementary Table 2**) from plasmid pIVEX-Fluc3xPro[7]. Samples have been incubated at 37°C for defined time periods. 1 µl of each reaction were added on to white 96-well chimney flat bottom microtiter plates. 40 µl of luminol substrate (Promega) were added, immediately before luminescence was detected using a Tecan Infinite M1000.

Negative-stain electron microscopy

Ribosomal particles were diluted in Buffer B to final concentrations of 4.0 A_{260}/ml up to 5.0 A_{260}/ml in order to determine the optimal ribosome density for cryo-EM. Samples were stained according with uranyl acetate. Micrographs were taken using a Morgagni transmission electron microscope (FEI), 80 kV, wide angle 1K CCD at direct magnifications of 72K.

Cryogrid preparation for the NlpD-PPP-SRC and NlpD-PP-SRC

Dataset 1: For grid preparation 4.5 OD A_{260}/ml monosomes of the full-length NlpD-PPP-SRC were used. Dataset 2: For grid preparation 5.0 OD A_{260}/ml monosomes of the full length NlpD-PPP-SRC were used and a 3x excess of modified EF-P over 70S was added and incubated for 20 mins at 37°C. Dataset 3: For grid preparation 4.5 OD A_{260}/ml monosomes of the truncated NlpD-PP SRC were used. A 5x excess of modified EF-P over 70S as well as 100 µM evernimicin (to ensure absence of A-site tRNA[47]) were added and incubated for 5 mins at 37°C. All samples were applied to 2 nm precoated Quantifoil R3/3 holey carbon supported grids and vitrified using a Vitrobot Mark IV (FEI company).

Ribosome complexes for kinetic experiments

The mRNA GGGCAAGGAGGUAAAUAAUGCCGCCGCCGUUCAUU) coding for fMPPPF was synthesized by IBA Lifescience. Initiation complexes were formed by incubating 70S ribosomes (1 µM) with IF 1, IF2, IF3 (1.5 µM each), f[^{3}H]Met-tRNA^{fMet} (3 µM) and GTP (1 mM) in buffer D (50 mM Tris-HCl, pH 7.5 at 37°C, 70 mM NH_4Cl,

30 mM KCl and 7 mM $MgCl_2$) for 30 min[5]. Initiation complexes were purified by centrifugation through a 400 µl sucrose cushion (40% sucrose in buffer D) at 260,000 g for 2 h at 4°C. Pellets were dissolved in buffer D, flash frozen and stored at -80°C. [^{14}C]Phe-tRNA^{Phe} was prepared from total tRNA as described. tRNA^{Pro} *in-vitro* transcripts were prepared and aminoacylated as described[5]. Ternary complexes EF-Tu–GTP–aminoacyl-tRNA were prepared by incubating aminoacyl-tRNA (Pro-tRNA^{Pro} and Phe-tRNA^{Phe}) with a 2.5-fold excess of EF-Tu, GTP (1 mM), pyruvate kinase (0.1 µg/µl) and phosphoenolpyruvate (3 mM) for 15 min at 37°C.

***In vitro* translation of fMPPPF model peptide**

Initiation complexes (0.2 µM), ternary complexes Pro and Phe (each 2 µM), EF-G (1 µM) and EF-P (varying concentrations) were mixed in buffer E (50 mM Tris-HCl, pH 7.5 at 37°C, 70 mM NH_4Cl, 30 mM KCl, 3.5 mM $MgCl_2$, 0.5 mM spermidine, 8 mM putrescine and 2 mM DTT) at 37°C. The reaction was quenched after 20 s with KOH (0.5 M), hydrolyzed for 30 min at 37°C and neutralized with glacial acetic acid. Amino acids and peptides were separated by reversed-phase HPLC (Chromolith® Performance RP8e 100-4.6 column, Merck) using a 0-65% acetonitrile gradient in 0.1% TFA. Products and educts were quantified by double-label scintillation counting[5].

Molecular Dynamics Simulations

To obtain the dynamics of the region surrounding the peptdidyl transferase center (PTC) in presence of EF-P, unmodified EF-P or without EF-P, we carried out all-atom explicit-solvent molecular dynamics (MD) simulations. The simulations were started (i) from the cryo-EM structure, (ii) from the cryo-EM structure after removal of the β-lysine modification of Lys34 (EF-P), and (iii) after removal of EF-P. Since the structural differences between the cryo-EM structures with and without EF-P are only found in the vicinity of the PTC, we used a reduced simulation system that allowed us to increase the achievable simulation time. The simulation system (+EF-P) includes all residues of the cryo-EM structure located within 35 Å of any atom of the P-site tRNA CCA-tail, of the attached peptide, or of the β-lysine modified Lys34 of EF-P. Nucleotides (amino acids) that are not within this radius, but whose 5'- and 3'- (n- and c-) neighbors are within the

radius, are also included in the simulation system. Nucleotides whose 5' (3') bound nucleotide neighbor is not in the simulation system were treated as 5' (3') terminal nucleotides. Any amino acid i whose i−1 neighbor (i + 1 neighbor) is not in the simulation system was capped by an uncharged N-terminal acetyl (C-terminal amide). Positions of residues in a 25 Å radius were not restrained (inner layer), while heavy atom positions the remaining residues (outer layer) were restrained by a harmonic potential. The harmonic force constant k of each restrained atom was chosen as k = 8RT πrmsf2 where rmsf is the root mean square fluctuation of the corresponding atom obtained from a 2 μs-simulations of the full ribosome in complex with A- and P-site tRNAs and the ErmBL peptide[28]. For those heavy atoms without corresponding atoms in the full-ribsome simulations, the average of all other force constants was used. Two more simulation systems were used, one after removal of the modification of EF-P Lys34 (+EF-P (unmod)) and the other after removal of all EF-P atoms (–EF-P). To place initial Mg ions, a cryo-EM structure of the ribosome[36] was aligned to each simulation system. Then, Mg ions resolved in the cryo-EM structure that are located within 5 Å of the atoms of the simulation system were extracted from the aligned structure and included in the simulations system. WHATIF[48] was used to determine the protonation states of the histidines. Each simulation systems was then solvated in a dodecahedron box of water molecules with a minimum distance of 1.5 nm between the atoms of the simulation system and the box boundaries using the program solvate[49]. To neutralize the overall charge of each system, first the Coulomb potential at the positions of all water oxygen atoms was calculated based on the charges and positions of all other atoms. Iteratively, the water molecule with the lowest Coulomb potential was replaced by a K^+ ion and the Coulomb potential at all other water oxygens was updated until the overall charge was neutral. Using the program GENION[49], subsequently 7 mM $MgCl_2$ and 150 mM KCl were added. All simulations were carried out with Gromacs 5[49] using the amberff12sb force field[50] and the SPC/E water model[51]. Force field parameters for modified nucleotides were taken from Aduri et al[52]. Potassium and chloride ion parameters were taken from Joung and Cheatham[53]. Atom types for β-lysine modified Lys were obtained with ANTECHAMBER[54] and partial charges were determined using DFT-B3LYP with a 6-31/G* basis set. The ester bond between the c-terminal proline and A76 of the P-site

tRNA was treated as described earlier[55]. LennardJones and short-range Coulomb interactions were calculated within a distance of 1 nm, while long-range Coulomb interactions were calculated using particle-mesh Ewald summation[56]. The LINCS algorithm was used to constrain bond lengths[57] and virtual site constraints[58] were used for hydrogens, allowing an integration time step of 4 fs. Solute and solvent temperatures were controlled independently at 300 K using velocity rescaling[59] with a coupling time constant of 0.1 ps. For each of the three simulation systems, the system was equilibrated in four steps. First, the potential energy was minimized using steepest decent while restraining the positions of all solute heavy atoms (k = 1000 kJ mol^{-1} nm^{-2}). Second, for the first 50 ns, the pressure was coupled to a Berendsen barostat (1 ps coupling time)[60] and position restraints were applied. Third, during the next 20 ns, the position restraint force constant was linearly decreased to the values obtained from the full-ribosome simulations for the outer-layer atoms and to zero for the remaining atoms. Finally, for production runs starting at 70 ns, the Parrinello-Rahman barostat was used[61]. At simulation times 170, 270, 370, and 470 ns coordinates were extracted from the trajectory, new velocities were assigned according to a Boltzmann distribution, and subsequently new simulations were started, resulting in a total of 15 simulations, 2 μs each, accumulating to a total production run simulation time of 30 μs.

Conformational landscape of CCA-end and C-terminal proline

To investigate how either the removal of the modification of EF-P or the removal of EF-P entirely changes the conformation of the P-site CCA-tail and the C-terminal proline of the peptide, we carried out a Principal Component Analysis (PCA)[44]. A PCA is used to extract the dominant modes of motion, here the first two eigenvectors. To that aim, we first aligned all the trajectories using all 23S P atoms and, second, extracted backbone atoms of the CCA-tail (O3', C3', C4', C5', O5', and P atoms) and of the peptide (N, CA, C, and O atoms). The extracted trajectories were then concatenated and the atomic displacement covariance matrix was calculated. The eigenvectors of this covariance matrix were sorted according to their eigenvalues. The eigenvectors corresponding to the largest eigenvalues represent the most dominant conformational modes. To describe the structural ensembles obtained from the three sets of simulations, first, the projection of all

the frames onto the first two eigenvectors was calculated. For each set of simulations, the projections were then sorted into 2-dimensional bins and the logarithm of the probability $\rho = c_{i,j}/c_{total}$ of each bin i,j was calculated, where $c_{i,j}$ is the number of the projections in the bin, c_{total} is the total number of frames (**Fig. 6a-c**). For comparison, our cryo-EM structure with EF-P as well the X-ray structures of the pre-attack conformation[29] and the uninduced and induced conformations[45] were projected onto the two conformational modes (**Fig. 6a-c**). For each set of simulations, all the structures sorted into the bin marked with a cross in the conformational landscape (**Fig. 6a-c**) were extracted. For each set, from the extracted structures the one with the median peptide bond distance was chosen and is shown in (**Fig. 6d-f**).

Cryo-electron microscopy and single particle reconstruction

Data collection were performed on FEI Titan Krios transmission electron microscopes equipped with a Falcon II direct electron detector (FEI) at 300 kV at a pixel size of 1.064 Å (Dataset 1) or 1.084 Å (Dataset 2 and 3). Dataset 1: Defocus range was from -1.0 to -2.5 µm (underfocus) resulting in 1156 Micrographs after manual inspection and discarding micrographs with resolution worse than 4 Å. Each micrograph contained 16 frames (2.68 $e^-/ Å^2$). Original image stacks were motion-corrected and dose weighted using MotionCor2[62]. Dataset 2 and 3: Defocus range was from -0.8 to -2.5 µm (underfocus) resulting in 2109 micrographs for Dataset 2 and 1957 micrographs for Dataset 3 after manual inspection and discarding micrographs showing a resolution worse than 3.3 Å (Dataset 2) and 3.4 Å (Dataset 3), respectively. Each micrograph contained 17 frames in total (2.4 $e^-/ Å^2$ + 4 $e^-/ Å^2$ pre exposure) and frames 0-9 were used resulting in a total dose of 28 $e^-/ Å^2$. Original image stacks were motion-corrected using MotionCor2[62]. Power-spectra, defocus values, astigmatism and estimation of resolution were determined using CTFFIND4 software[63].

After automated particle picking using SIGNATURE[64] single particles were processed using RELION-2[65]. All particles from the three datasets (Dataset 1: 121,704 particles, Dataset 2: 229,613 particles, Dataset 3: 229,458 particles) were first subjected to 3D refinement using an *E. coli* 70S ribosome as reference structure and subsequently a 3D classification was performed (**Supplementary Fig. 1**). Dataset 1 was classified into

four classes and dataset 2 and 3 into eight classes. For dataset 3 classes 2 and 3 were joined and a second classification was performed with a mask focusing on EF-P. Final structures of all datasets were refined, corrected for the modulation transfer function of the Falcon 2 detector and sharpened by applying a negative B-factor automatically estimated by RELION-2 (**Table 1**). Resolution was estimated using the "gold standard" criterion (FSC=0.143).

Molecular modeling and map-docking procedures

The molecular model for the ribosomal proteins and rRNA of either the PPP or PP stalled complexes is based on the molecular model for the 70S subunit from the cryo-EM reconstruction of the *E. coli* 70S ribosome (PDB ID 5AFI)[36] and obtained by performing a rigid body fit into the cryo-EM density map of the corresponding stalled complex using UCSF Chimera[66] (fit in map function). For *E. coli* EF-P, a homology model was generated using HHPred[67] based on a template from *T. thermophilus* (PDB ID 3HUW)[22]. The model was fitted to the density using Chimera[66] and refined in Coot[68]. The post-translational modification of ε(R)–β–lysyl-hydroxylysine that is positioned at K34 of EF-P was designed using Chem3DPro (PerkinElmer), manually placed into the cryo-EM density map at position 34 of EF-P and refined in Coot. P-site tRNA of the *E. coli* 70S ribosome (PDB ID 5AFI)[36] was manually mutated to $tRNA^{Pro(CCG)}$. In the case of the truncated PP-SRC in the presence of EF-P, the L1 stalk and L1 protein were taken from the crystal structure of *T. thermophilus* (PDB ID 3HUW), manually mutated and refined using Coot. Nucleotides of the PTC that differ from the cryo-EM *E. coli* 70S ribosome (PDB ID 5AFI)[36] were manually refined into density using Coot. Atomic coordinates were refined using *phenix.real_space_refine*,[69] with restraints obtained by *phenix.secondary_structure_restraints*.[69] Cross-validation against overfitting was performed as described elsewhere[70]. Statistics of the refined models were obtained using MolProbity[71] and are presented in **Table 1**.

Figure preparation

Figures showing electron densities and atomic models were generated using either UCSF Chimera or PyMol Molecular Graphic Systems (Version 1.8 Schrödinger).

REFERENCES (up to 60 references)

1. Pavlov, M.Y. et al. Slow peptide bond formation by proline and other N-alkylamino acids in translation. *Proc Natl Acad Sci U S A* **106**, 50-4 (2009).
2. Johansson, M. et al. pH-sensitivity of the ribosomal peptidyl transfer reaction dependent on the identity of the A-site aminoacyl-tRNA. *Proc. Natl Acad. Sci. USA* **108**, 79-84 (2011).
3. Muto, H. & Ito, K. Peptidyl-prolyl-tRNA at the ribosomal P-site reacts poorly with puromycin. *Biochem. Biophys. Res. Commun.* **366**, 1043-7 (2008).
4. Wohlgemuth, I., Brenner, S., Beringer, M. & Rodnina, M.V. Modulation of the rate of peptidyl transfer on the ribosome by the nature of substrates. *J. Biol. Chem.* **283**, 32229-35 (2008).
5. Doerfel, L.K. et al. EF-P is essential for rapid synthesis of proteins containing consecutive proline residues. *Science* **339**, 85-8 (2013).
6. Doerfel, L.K. et al. Entropic Contribution of Elongation Factor P to Proline Positioning at the Catalytic Center of the Ribosome. *J Am Chem Soc* **137**, 12997-3006 (2015).
7. Ude, S. et al. Translation elongation factor EF-P alleviates ribosome stalling at polyproline stretches. *Science* **339**, 82-5 (2013).
8. Woolstenhulme, C.J. et al. Nascent peptides that block protein synthesis in bacteria. *Proc Natl Acad Sci U S A* **110**, E878-87 (2013).
9. Gutierrez, E. et al. eIF5A promotes translation of polyproline motifs. *Mol Cell* **51**, 35-45 (2013).
10. Dever, T.E., Gutierrez, E. & Shin, B.S. The hypusine-containing translation factor eIF5A. *Crit Rev Biochem Mol Biol*, 1-13 (2014).
11. Lassak, J., Wilson, D.N. & Jung, K. Stall no more at polyproline stretches with the translation elongation factors EF-P and IF-5A. *Mol Microbiol* (2015).
12. Peil, L. et al. Distinct XPPX sequence motifs induce ribosome stalling, which is rescued by the translation elongation factor EF-P. *Proc Natl Acad Sci U S A* **110**, 15265-70 (2013).
13. Behshad, E. et al. Enantiomeric free radicals and enzymatic control of stereochemistry in a radical mechanism: the case of lysine 2,3-aminomutases. *Biochemistry* **45**, 12639-46 (2006).
14. Yanagisawa, T., Sumida, T., Ishii, R., Takemoto, C. & Yokoyama, S. A paralog of lysyl-tRNA synthetase aminoacylates a conserved lysine residue in translation elongation factor P. *Nat. Struct. Mol. Biol.* **17**, 1136-43 (2010).
15. Navarre, W.W. et al. PoxA, yjeK, and elongation factor P coordinately modulate virulence and drug resistance in *Salmonella enterica*. *Mol. Cell* **39**, 209-221 (2010).
16. Peil, L. et al. Lys34 of translation elongation factor EF-P is hydroxylated by YfcM. *Nat. Chem. Biol.* **8**, 695-7 (2012).
17. Bailly, M. & de Crecy-Lagard, V. Predicting the pathway involved in post-translational modification of elongation factor P in a subset of bacterial species. *Biol. Direct* **5**, 3 (2010).
18. Lassak, J. et al. Arginine-rhamnosylation as new strategy to activate translation elongation factor P. *Nat Chem Biol* **11**, 266-70 (2015).

19. Rajkovic, A. et al. Cyclic Rhamnosylated Elongation Factor P Establishes Antibiotic Resistance in Pseudomonas aeruginosa. *MBio* **6**, e00823 (2015).
20. Rajkovic, A. et al. Translation Control of Swarming Proficiency in Bacillus subtilis by 5-Amino-pentanolylated Elongation Factor P. *J Biol Chem* **291**, 10976-85 (2016).
21. Hanawa-Suetsugu, K. et al. Crystal structure of elongation factor P from *Thermus thermophilus* HB8. *Proc. Natl Acad. Sci. U S A* **101**, 9595-9600 (2004).
22. Blaha, G., Stanley, R.E. & Steitz, T.A. Formation of the first peptide bond: the structure of EF-P bound to the 70S ribosome. *Science* **325**, 966-70 (2009).
23. Melnikov, S. et al. Crystal Structure of Hypusine-Containing Translation Factor eIF5A Bound to a Rotated Eukaryotic Ribosome. *J Mol Biol* **428**, 3570-3576 (2016).
24. Schmidt, C. et al. Structure of the hypusinylated eukaryotic translation factor eIF-5A bound to the ribosome. *Nucleic Acids Res* **44**, 1944-51 (2016).
25. Starosta, A.L. et al. Translational stalling at polyproline stretches is modulated by the sequence context upstream of the stall site. *Nucleic Acids Res* **42**, 10711-9 (2014).
26. Arenz, S. et al. Drug Sensing by the Ribosome Induces Translational Arrest via Active Site Perturbation. *Mol Cell* **56**, 446-52 (2014).
27. Arenz, S. et al. Molecular basis for erythromycin-dependent ribosome stalling during translation of the ErmBL leader peptide. *Nat Commun* **5**, 3501 (2014).
28. Arenz, S. et al. A combined cryo-EM and molecular dynamics approach reveals the mechanism of ErmBL-mediated translation arrest. *Nature communications* **7**, 12026 (2016).
29. Polikanov, Y.S., Steitz, T.A. & Innis, C.A. A proton wire to couple aminoacyl-tRNA accommodation and peptide-bond formation on the ribosome. *Nat Struct Mol Biol* **21**, 787-93 (2014).
30. Voorhees, R.M., Weixlbaumer, A., Loakes, D., Kelley, A.C. & Ramakrishnan, V. Insights into substrate stabilization from snapshots of the peptidyl transferase center of the intact 70S ribosome. *Nat Struct Mol Biol* **16**, 528-533 (2009).
31. Katoh, T., Wohlgemuth, I., Nagano, M., Rodnina, M.V. & Suga, H. Essential structural elements in tRNA(Pro) for EF-P-mediated alleviation of translation stalling. *Nat Commun* **7**, 11657 (2016).
32. Schuller, A.P., Wu, C.C., Dever, T.E., Buskirk, A.R. & Green, R. eIF5A Functions Globally in Translation Elongation and Termination. *Mol Cell* **66**, 194-205 e5 (2017).
33. Pelechano, V. & Alepuz, P. eIF5A facilitates translation termination globally and promotes the elongation of many non polyproline-specific tripeptide sequences. *Nucleic Acids Res* (2017).
34. Zhou, J., Korostelev, A., Lancaster, L. & Noller, H.F. Crystal structures of 70S ribosomes bound to release factors RF1, RF2 and RF3. *Curr Opin Struct Biol* **22**, 733-42 (2012).
35. Melnikov, S. et al. Molecular insights into protein synthesis with proline residues. *EMBO Rep* **17**, 1776-1784 (2016).
36. Fischer, N. et al. Structure of the E. coli ribosome-EF-Tu complex at <3 A resolution by C-corrected cryo-EM. *Nature* **520**, 567-570 (2015).

37. Seefeldt, A.C. et al. The proline-rich antimicrobial peptide Onc112 inhibits translation by blocking and destabilizing the initiation complex. *Nat Struct Mol Biol* **22**, 470-5 (2015).
38. Roy, R.N., Lomakin, I.B., Gagnon, M.G. & Steitz, T.A. The mechanism of inhibition of protein synthesis by the proline-rich peptide oncocin. *Nat Struct Mol Biol* **22**, 466-9 (2015).
39. Matheisl, S., Berninghausen, O., Becker, T. & Beckmann, R. Structure of a human translation termination complex. *Nucleic acids Res.* **43**, 8615-26 (2015).
40. Bischoff, L., Berninghausen, O. & Beckmann, R. Molecular basis for the ribosome functioning as an L-tryptophan sensor. *Cell Rep* **9**, 469-75 (2014).
41. Su, T. et al. The force-sensing peptide VemP employs extreme compaction and secondary structure formation to induce ribosomal stalling. *Elife* **6**(2017).
42. Sohmen, D. et al. Structure of the Bacillus subtilis 70S ribosome reveals the basis for species-specific stalling. *Nat Commun* **6**, 6941 (2015).
43. Zhang, J. et al. Mechanisms of ribosome stalling by SecM at multiple elongation steps. *eLife* **4**(2015).
44. Amadei, A., Linssen, A.B. & Berendsen, H.J. Essential dynamics of proteins. *Proteins* **17**, 412-25 (1993).
45. Schmeing, T.M., Huang, K.S., Strobel, S.A. & Steitz, T.A. An induced-fit mechanism to promote peptide bond formation and exclude hydrolysis of peptidyl-tRNA. *Nature* **438**, 520-524 (2005).
46. Arenz, S., Nguyen, F., Beckmann, R. & Wilson, D.N. Cryo-EM structure of the tetracycline resistance protein TetM in complex with a translating ribosome at 3.9-A resolution. *Proc Natl Acad Sci U S A* **112**, 5401-6 (2015).
47. Arenz, S. et al. Structures of the orthosomycin antibiotics avilamycin and evernimicin in complex with the bacterial 70S ribosome. *Proc Natl Acad Sci U S A* **113**, 7527-32 (2016).
48. Vriend, G. WHAT IF: a molecular modeling and drug design program. *J Mol Graph* **8**, 52-6, 29 (1990).
49. Pronk, S. et al. GROMACS 4.5: a high-throughput and highly parallel open source molecular simulation toolkit. *Bioinformatics* **29**, 845-54 (2013).
50. Lindorff-Larsen, K. et al. Improved side-chain torsion potentials for the Amber ff99SB protein force field. *Proteins* **78**, 1950-8 (2010).
51. Berendsen, H.J.C., Grigera, J.R. & Straatsma, T.P. The missing term in effective pair potentials. *J. Phys. Chem.* **91**, 6269–6271 (1987).
52. Aduri, R. et al. AMBER Force Field Parameters for the Naturally Occurring Modified Nucleosides in RNA. *J Chem Theory Comput* **3**, 1464-75 (2007).
53. Joung, I.S. & Cheatham, T.E., 3rd. Determination of alkali and halide monovalent ion parameters for use in explicitly solvated biomolecular simulations. *J Phys Chem B* **112**, 9020-41 (2008).
54. Wang, J., Wang, W., Kollman, P.A. & Case, D.A. Automatic atom type and bond type perception in molecular mechanical calculations. *J Mol Graph Model* **25**, 247-60 (2006).
55. Bock, L.V. et al. Energy barriers and driving forces in tRNA translocation through the ribosome. *Nat Struct Mol Biol* **20**, 1390-6 (2013).

56. Essmann, U. et al. A smooth particle mesh ewald method. *J. Chem. Phys.* **103**, 8577–8593 (1995).
57. Hess, B. P-LINCS: A Parallel Linear Constraint Solver for Molecular Simulation. *J Chem Theory Comput* **4**, 116-22 (2008).
58. Feenstra, K.A., Hess, B. & Berendsen, H.J.C. Improving efficiency of large time-scale molecular dynamics simulations of hydrogen-rich systems. *J. Comput. Chem.* **20**, 786–798 (1999).
59. Bussi, G., Donadio, D. & Parrinello, M. Canonical sampling through velocity rescaling. *J Chem Phys* **126**, 014101 (2007).
60. Berendsen, H.J.C., Postma, J.P.M., van Gunsteren, W.F., DiNola, A. & Haak, J.R. Molecular dynamics with coupling to an external bath. *J. Chem. Phys.* **81**(1984).
61. Parrinello, M. & Rahman, A. Polymorphic transitions in single crystals: A new molecular dynamics method. *J. Appl. Phys.* **52**(1981).
62. Zheng, S.Q. et al. MotionCor2: anisotropic correction of beam-induced motion for improved cryo-electron microscopy. *Nat Methods* **14**, 331-332 (2017).
63. Rohou, A. & Grigorieff, N. CTFFIND4: Fast and accurate defocus estimation from electron micrographs. *J Struct Biol* **192**, 216-21 (2015).
64. Chen, J.Z. & Grigorieff, N. SIGNATURE: a single-particle selection system for molecular electron microscopy. *J. Struct. Biol.* **157**, 168-73 (2007).
65. Scheres, S.H. RELION: implementation of a Bayesian approach to cryo-EM structure determination. *J Struct Biol* **180**, 519-30 (2012).
66. Pettersen, E.F. et al. UCSF Chimera - A Visualization System for Exploratory Research and Analysis. *J. Comput. Chem.* **25**, 1605-1612 (2004).
67. Hildebrand, A., Remmert, M., Biegert, A. & Soding, J. Fast and accurate automatic structure prediction with HHpred. *Proteins* **77 Suppl 9**, 128-132 (2009).
68. Emsley, P. & Cowtan, K. Coot: Model-Building Tools for Molecular Graphics. *Acta Crystallographica Section D - Biological Crystallography* **60**, 2126-2132 (2004).
69. Adams, P.D. et al. PHENIX: a comprehensive Python-based system for macromolecular structure solution. *Acta Crystallogr D Biol Crystallogr* **66**, 213-21 (2010).
70. Brown, A. et al. Tools for macromolecular model building and refinement into electron cryo-microscopy reconstructions. *Acta Crystallogr D Biol Crystallogr* **71**, 136-53 (2015).
71. Chen, V.B. et al. MolProbity: all-atom structure validation for macromolecular crystallography. *Acta Crystallogr D Biol Crystallogr* **66**, 12-21 (2010).

ACKNOWLEDGMENTS

We thank Susanne Rieder and Olaf Geintzer for expert technical assistance and Bertrand Beckert for helpful comments. This research was supported by iNEXT project 1503 (to D.N.W.) and grants of the Forschergruppe FOR1805 (to A.V., D.N.W., H.G, I.W, M.V.R and R.B.) from the Deutsche Forschungsgemeinschaft (DFG).

AUTHOR CONTRIBUTIONS

P.H., S.A., M.G., A.H., J.N., O.B., R.B., D.N.W. performed cryo-EM analysis, P.H. performed Fluc assays, P.H., M.G., L.P., A.L.S, T.T. prepared active EF-P proteins, J.O.F, I.W., F.P., M.V.R. performed peptide synthesis assays, L.V.B., H.G., A.C.V. performed molecular dynamic simulations. P.H. and D.N.W. prepared the figures and wrote the paper with help from I.W., L.V.B, A.C.V., and M.V.R.

COMPETING FINANCIAL INTERESTS

The authors declare no competing financial interests.

ACCESSION NUMBERS

The cryo-EM maps and associated atomic coordinates have been deposited in the EMDB and PDB with the accession codes EMDB-XYZ/PDB-XYZ (Dataset 1, P-site tRNA only), EMDB-XYZ/PDB-XYZ (Dataset 1, A- and P-site tRNAs), EMDB-XYZ/PDB-XYZ (Dataset 2, P-site tRNA only), EMDB-XYZ/PDB-XYZ (Dataset 2, A- and P-site tRNA and EF-P), EMDB-XYZ/PDB-XYZ (Dataset 3, P- and E-site tRNAs), EMDB-XYZ/PDB-XYZ (Dataset 3, P-site tRNA and EF-P).

FIGURES (Figure legends should be <300 words each.)

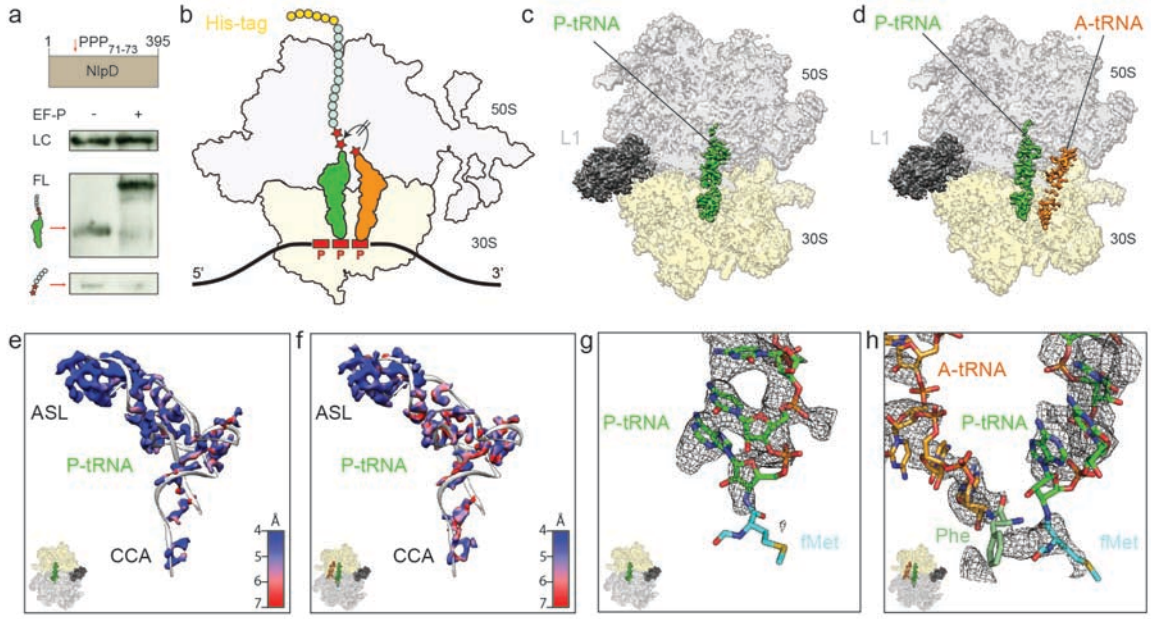

Figure 1 Cryo-EM structures of polyproline-stalled ribosomes in the absence of EF-P. (**a**) Schematic representation of NlpD-PPP reporter protein (brown) with the site of the PPP-motif indicated. Western blot using an anti-HA-tag antibody of *in vitro* translation reactions of NlpD-PPP reporter in the absence (-) and presence (+) of EF-P. Full-length (FL), peptidyl-tRNA and free peptide, as well as loading control (LC) are indicated. (**b**) Schematic representation and (**c-d**) cryo-EM reconstructions of PPP-stalled ribosome complexes formed in the absence of EF-P. (**e,f**) Cryo-EM density at high threshold (7σ), colored according to the local resolution, for the P-site tRNA (grey ribbon) from cryo-EM maps in (**c**) and (**d**), respectively. (**g**) Cryo-EM density (mesh) of the CCA-end of the P-site tRNA (green) from (**c**), with modeled fMet (cyan, PDB ID 1VY4)[29] illustrating lack of density for nascent chain even at low thresholds (4σ). (**h**) Cryo-EM density (mesh) of the CCA-end of the A-site tRNA (orange) and P-site tRNA (green) from (**d**), with modeled Phe (green) and fMet (cyan, PDB ID 1VY4)[29].

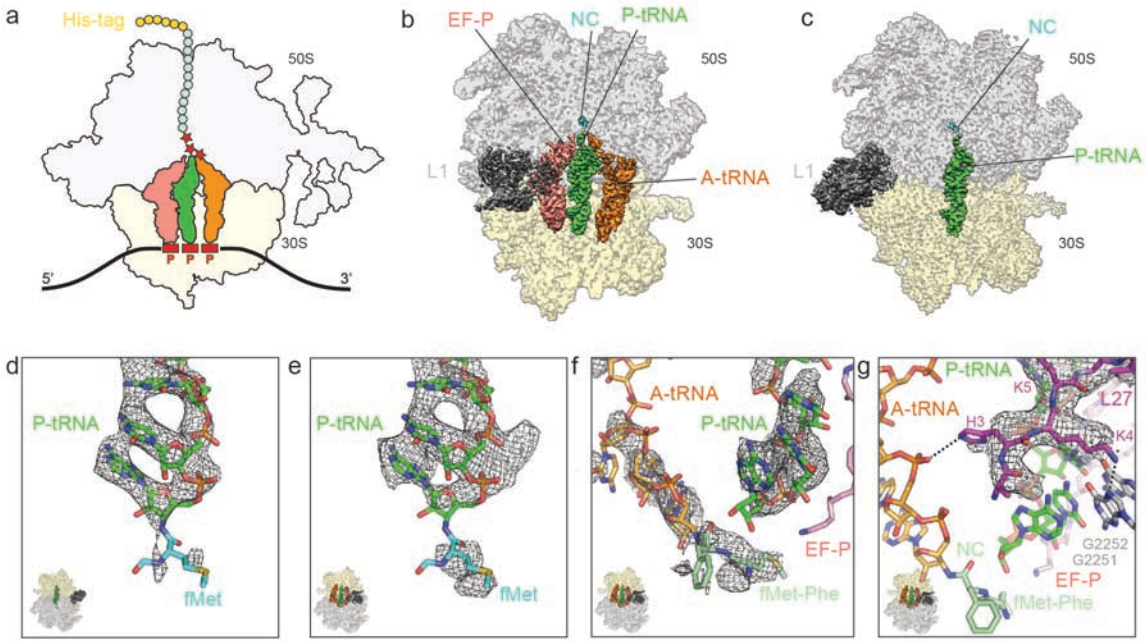

Figure 2 Cryo-EM structures of polyproline-stalled ribosomes in the presence of EF-P. (**a**) Schematic representation and (**b,c**) cryo-EM reconstructions of PPP-stalled ribosome complexes with (b) or without (c) of EF-P (salmon) bound in the E-site. (**d,e**) Cryo-EM density (mesh) of the CCA-end of the P-site tRNA (green) from (**c**) and (**b**), respectively, with modeled fMet (cyan, PDB ID 1VY4)[29]. (**f**) Cryo-EM density (mesh) of the CCA-end of the A-site tRNA (orange) and P-site tRNA (green) from (**b**), with modeled fMet-Phe dipeptide (green, PDB ID 1VY5)[29]. (**g**) Cryo-EM density (mesh) for the N-terminal residues of L27 (purple) showing possible interactions with residues G2251 and G2252 of the P-loop (grey) and A-site tRNA (orange).

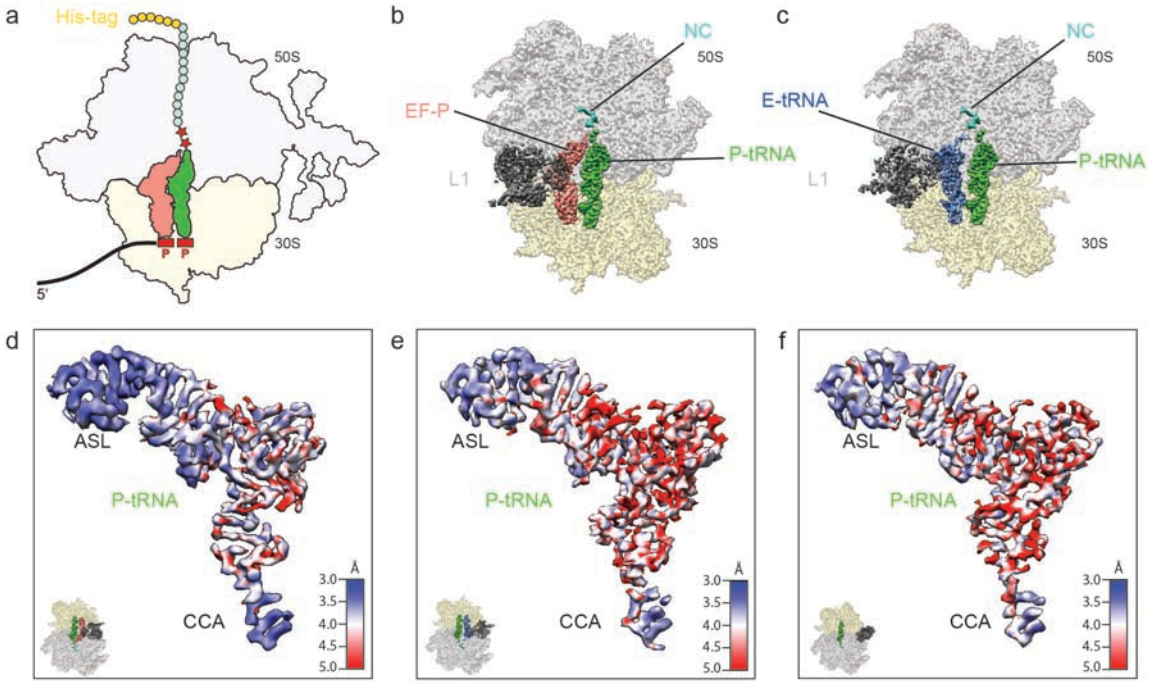

Figure 3 Stabilization of the P-site peptidyl-tRNA by EF-P. (**a**) Schematic representation and (**b,c**) cryo-EM reconstructions of truncated NlpD-PP-stalled ribosomes in the presence (**b**) or absence (**c**) of EF-P (salmon). (**d-f**) Cryo-EM densities colored according to local resolution for the P-site tRNAs from (**d**,**e**) reconstructions illustrated in (**b**,**c**), respectively, as well as from (**f**) the reconstruction from Fig. 2c.

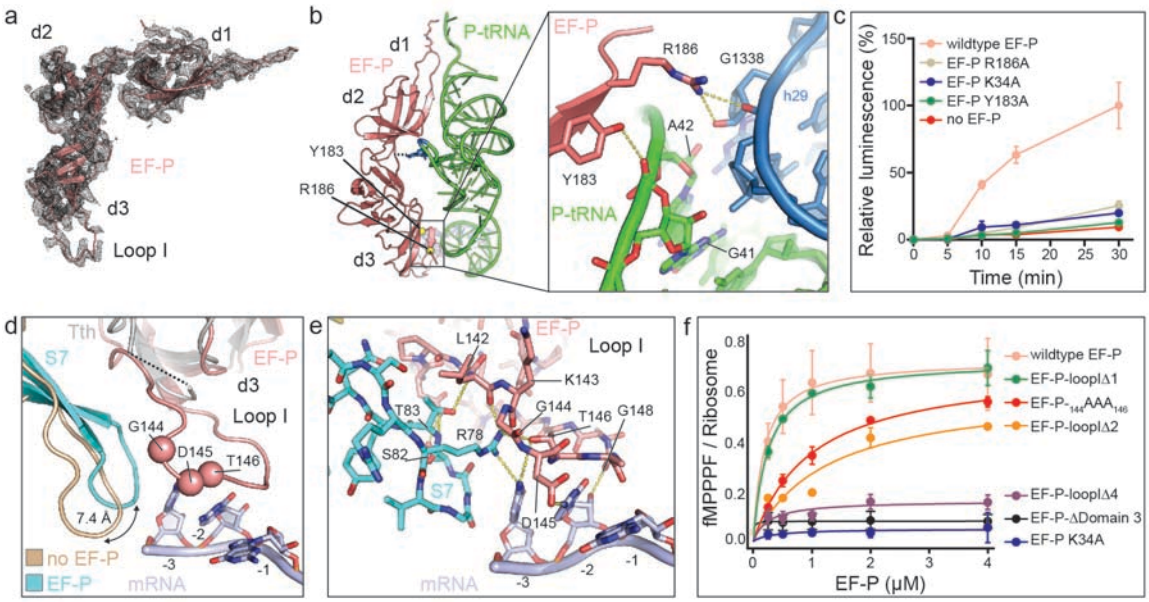

Figure 4 Interaction of EF-P with the P-site tRNA. (**a**) Cryo-EM density (mesh) with molecular model for EF-P (salmon ribbon) with domains 1-3 (d1-d3) indicated. (**b**) Overview of EF-P relative to P-site bound $tRNA^{Pro}$ (green) with a zoom on the interactions between Y183 and R186 of EF-P and their respective interaction partners of $tRNA^{Pro}$ and h29 (blue) of the 30S subunit. (**c**) Luminescence resulting from *in vitro* translated Fluc-3xPro was monitored over time and quantified in the absence of EF-P (red) or presence of wildtype EF-P (pink) or indicated EF-P variants. 100% luminescence is defined as the luminescence produced by Fluc-3xPro after a 30-min incubation in the presence of wildtype EF-P. Error bars represent the standard deviation of three independent experiments. (**d**) Location of EF-P d3 loop I relative to peptidyl-$tRNA^{Pro}$ (green) in the P-site, mRNA (light blue) and ribosomal protein S7 (cyan), with the position of the loop of S7 in the absence of EF-P (tan) indicated for reference. The relative position of *T. thermophilus* EF-P[22] (grey) is shown with the disordered region of d3 loop of EF-P indicated (dashed line). The positions of the conserved residues within the $_{144}GDT_{146}$ motif within loop I of EF-P are indicated by spheres. (**e**) Potential hydrogen-bond interactions (dashed yellow lines) between Loop I of EF-P (salmon), the E-site codon (blue) and S7 (cyan). (**f**) Synthesis of the fMPPPF peptide as a function of EF-P concentration, in the presence of wildtype EF-P (pink) or various EF-P variants. Error bars represent the standard deviation of three independent experiments.

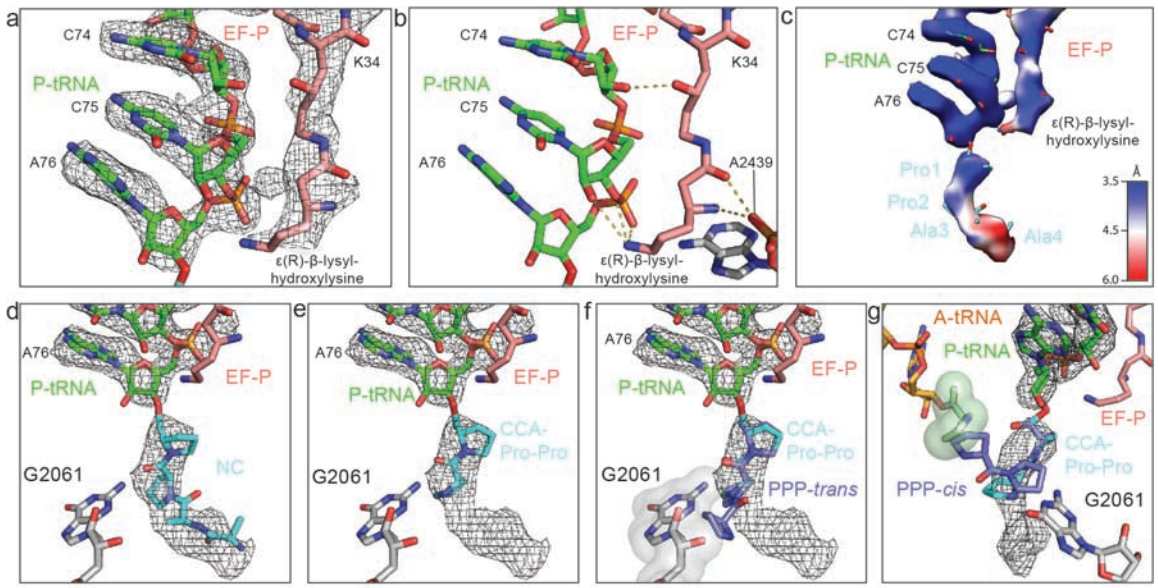

Figure 5 EF-P stabilizes the PP-containing nascent chain. (**a**) Cryo-EM density (grey mesh) for the CCA-end of the P-site tRNA (green) and ε(R)-β-lysyl-hydroxylysine modification of EF-P (salmon). (**b**) Same as (a), but without cryo-EM density, and potential hydrogen bond interactions (dashed lines) between the ε(R)-β-lysyl-hydroxylysine modification, P-site tRNA (green) and A2439 (grey) are indicated. (**c**) Cryo-EM density colored according to the local resolution for the CCA-end of the P-site tRNA, ε(R)-β-lysyl-hydroxylysine modification of EF-P and the modeled nascent chain (Pro1-Pro2-Ala3-Ala4). (**d-g**) Cryo-EM density (mesh) for the P-site tRNA with (d) the first four residues of the modeled nascent chain (NC) Pro1-Pro2-Ala3-Ala4 (cyan), (**e**) *all-trans* Pro-Pro conformation of CCA-Pro-Pro tRNA mimic in complex with yeast 80S ribosome (PDB ID 5DGV)[35], (**f**) three prolines of a polyproline type II (P_{II}) helix (PP-*trans*) modeled onto CCA-end of the P-site tRNA, with G2061 shown as a surface to better illustrate the steric clash with the PP-*trans* nascent chain, (**g**) three prolines of a polyproline type I (P_I) helix (PP-*cis*) modeled onto CCA-end of the P-site tRNA, showing a potential clash with a Pro residue (light green surface) attached to the A-site tRNA (orange).

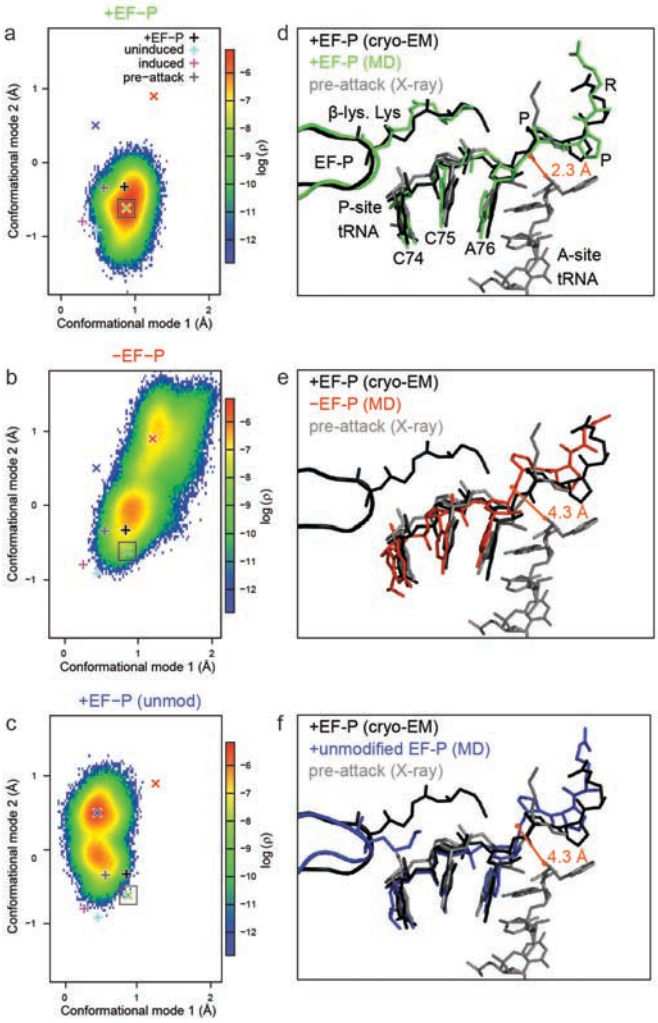

Figure 6 MD simulations of polyproline-stalled ribosomes in the presence and absence of EF-P. (**a-c**) Conformational landscape explored by MD simulations with (**a**) EF-P, (**b**) without EF-P, or (**c**) with unmodified EF-P. The logarithm of the probability density ρ is shown along the two most dominant conformational modes of the CCA-end and the C-terminal proline backbone atoms. Probability density maxima are indicated by crosses, green (simulations with EF-P), red (without EF-P) and blue (unmodified EF-P). For comparison, + signs indicate the projections of our cryo-EM derived structure (black), the pre-attack state[29] (grey), the uninduced and the induced states[45] (cyan and magenta, respectively). (**d-f**) Conformations of P-site tRNA with peptide and EF-P corresponding to the density maxima obtained from MD simulations (**d**) with EF-P (green), (**e**) without EF-P (red) and (**f**) with unmodified EF-P (blue). The cryo-EM structure with EF-P (black) and the pre-attack[29] (grey) conformation are shown for comparison.

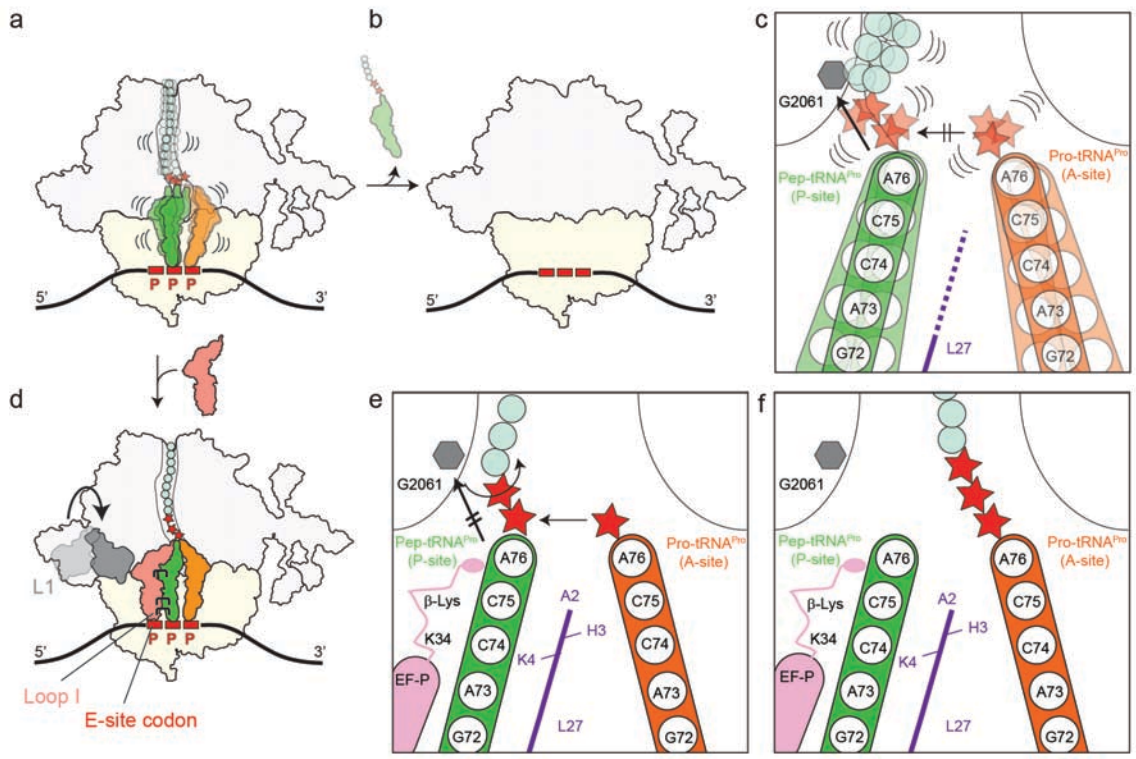

Figure 7 Mechanism of action of EF-P on polyproline stalled ribosomes. (**a**) Ribosomes stall during translation of proteins containing three consecutive prolines[5,7] leading to destabilization of the peptidyl-tRNA in the P-site, which (**b**) leads to peptidyl-tRNA drop-off, particular with short peptidyl-tRNAs[5]. (**c**) The *all-trans* or *all-cis* conformation of polyprolines (red stars) of the nascent chain is not possible because of a steric clash with G2061 (grey) within the tunnel wall, leading to peptidyl-tRNA destabilization and thus preventing accommodation of the A-site tRNA and peptide bond formation. (**d**) Ribosomes stalled on polyproline stretches are recognized by EF-P, which binds within the E-site region and stabilizes the peptidyl-tRNA. EF-P binding is facilitated via contacts with the L1 stalk[22] and the P-site tRNA[31] as well as E-site codon. (**e**) Interaction of the ε(R)-β-lysyl-hydroxylysine with the CCA-end of P-site $tRNA^{Pro}$ stabilizes the P-site tRNA as well as the nascent chain, by forcing the prolines to adopt an alternative conformation that passes into the ribosomal exit tunnel. (**f**) Thus, an optimal geometry between the nascent chain and the aminoacyl-tRNA in the A-site is achieved and peptide bond formation can occur.

Table 1 Cryo-EM data collection, refinement and validation statistics

	#1 P-site tRNA only (EMD ID xxxx, PDB xxxx)	#2 A- and P-site tRNA + EF-P (EMD ID xxxx PDB xxxx)	#3 P-site tRNA + EF-P
Data collection			
Microscope	FEI Titan Krios	FEI Titan Krios	FEI Titan Krios
Camera	Falcon II	Falcon II	Falcon II
Magnification	129,151	129,151	129,151
Voltage (kV)	300	300	300
Electron dose (e^{-}/Å^2)	28	28	28
Defocus range (μm)	-0.8 to -2.5	-0.8 to -2.5	-0.8 to -2.5
Pixel size (Å)	1.084	1.084	1.084
Initial particles (no.)	229,613	229,613	229,455
Final particles (no.)	75,089	21,655	69,761
Model composition			
Protein residues	5,531	5,951	5,944
RNA bases	4,547	4,693	4,613
Refinement			
Resolution range (Å)	3.3	3.9	3.2
Map CC (around atoms)	0.78	0.72	0.80
Map CC (whole unit cell)	0.76	0.75	0.75
$FSC_{average}$	0.85	0.85	0.85
Map sharpening *B* factor (Å^2)	-62,88	-66,61	-60,10
R.m.s. deviations			
Bond lengths (Å)	0.011	0.003	0.007
Bond angles (°)	0.729	0.594	0.932
Validation			
MolProbity score	1.77	1.64	1.77
Clashscore	4.29	3.44	4.11
Poor rotamers (%)	0	0.04	0.41
Ramachandran plot			
Favored (%)	92.06	91.33	88.83
Allowed (%)	7.76	8.37	10.74
Disallowed (%)	0.18	0.31	0.43

SUPPLEMENTARY FIGURES

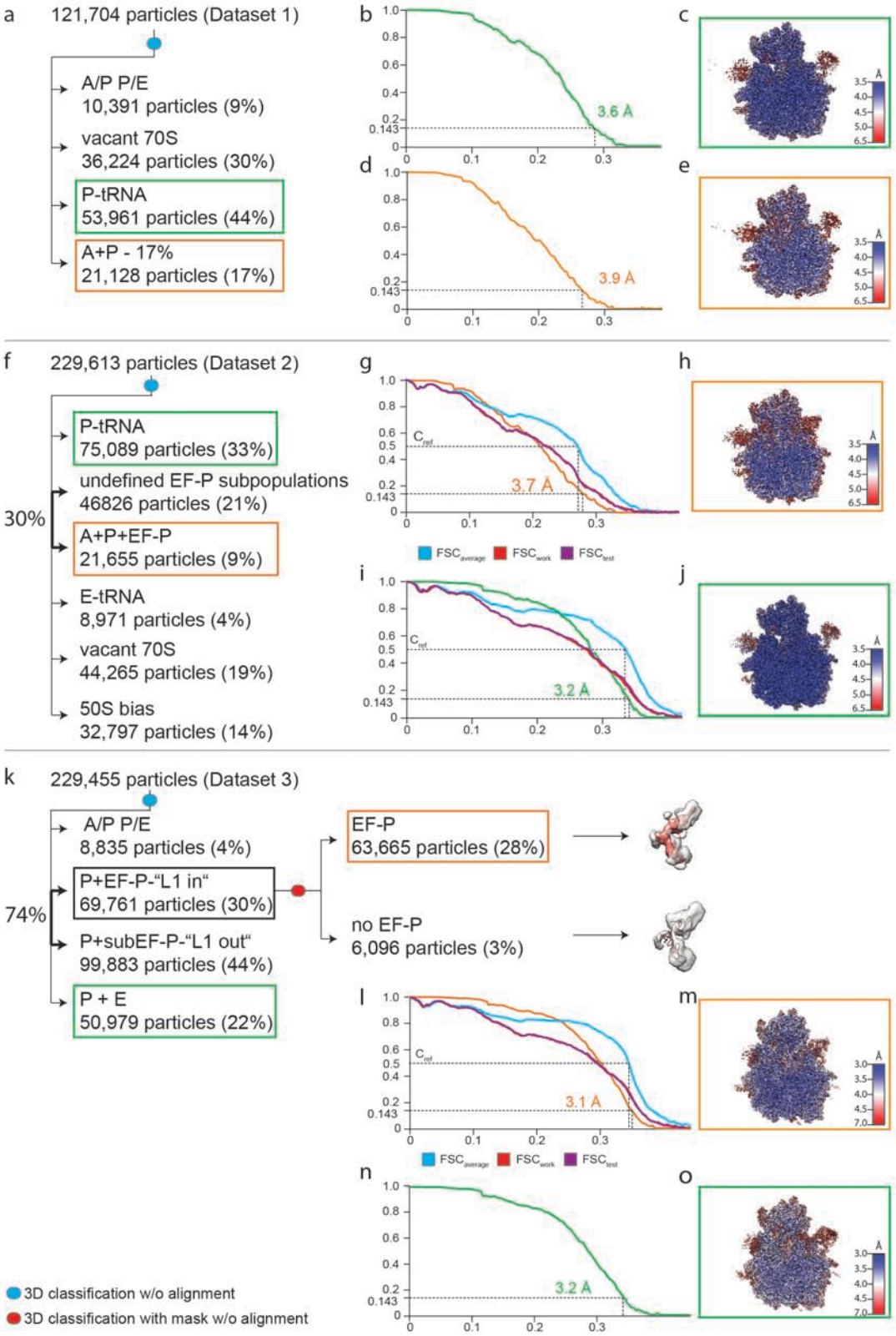

Figure S1 Data processing of the cryo-EM structures of polyproline-stalled ribosomes ± EF-P. (**a**) *In silico* sorting procedure for Dataset 1 derived from the PPP-stalled ribosome complexes prepared in the absence of EF-P. (**b**) Fourier-shell-correlation (FSC) curve (green) and (**c**) transverse section of the P-site tRNA only structure colored according to local resolution. (**d**) FSC curve (orange) and (**e**) transverse section of the A- and P-site tRNAs containing structure colored according to local resolution. In (b) and (d), the resolution at FSC=0.143 is indicated with a dashed line. (**f**) *In silico* sorting procedure for Dataset 2 derived from the PPP-SRC prepared in the presence of EF-P. (**g**) FSC curve (orange), as well as self and cross-validated correlations FSC_{work} (red) and FSC_{test} (purple), respectively. The resolutions at FSC=0.143 and FSC=0.5 (C_{ref}) are indicated with dashed lines. (**h**) Transverse section of the A- and P-site tRNA- and EF-P-containing structure colored according to local resolution. (**i**) FSC curve (green), as well as self and cross-validated correlations as in (**g**) but for the P-site tRNA only structure. (**j**) as (**h**) but for P-site tRNA only structure. (**k**) *In silico* sorting procedure for Dataset 3 derived from the PP-SRC prepared in the presence of EF-P. (**l**) FSC curve (orange), as well as self and cross-validated correlations FSC_{work} (red) and FSC_{test} (purple), respectively. The resolutions at FSC=0.143 and FSC=0.5 (C_{ref}) are indicated with dashed lines. (**m**) Transverse section of the P-site tRNA and EF-P structure colored according to local resolution. (**n**) FSC curve (green) for the P- and E-site tRNA containing structure. (**o**) as (**m**) but for P- and E-site tRNA containing structure.

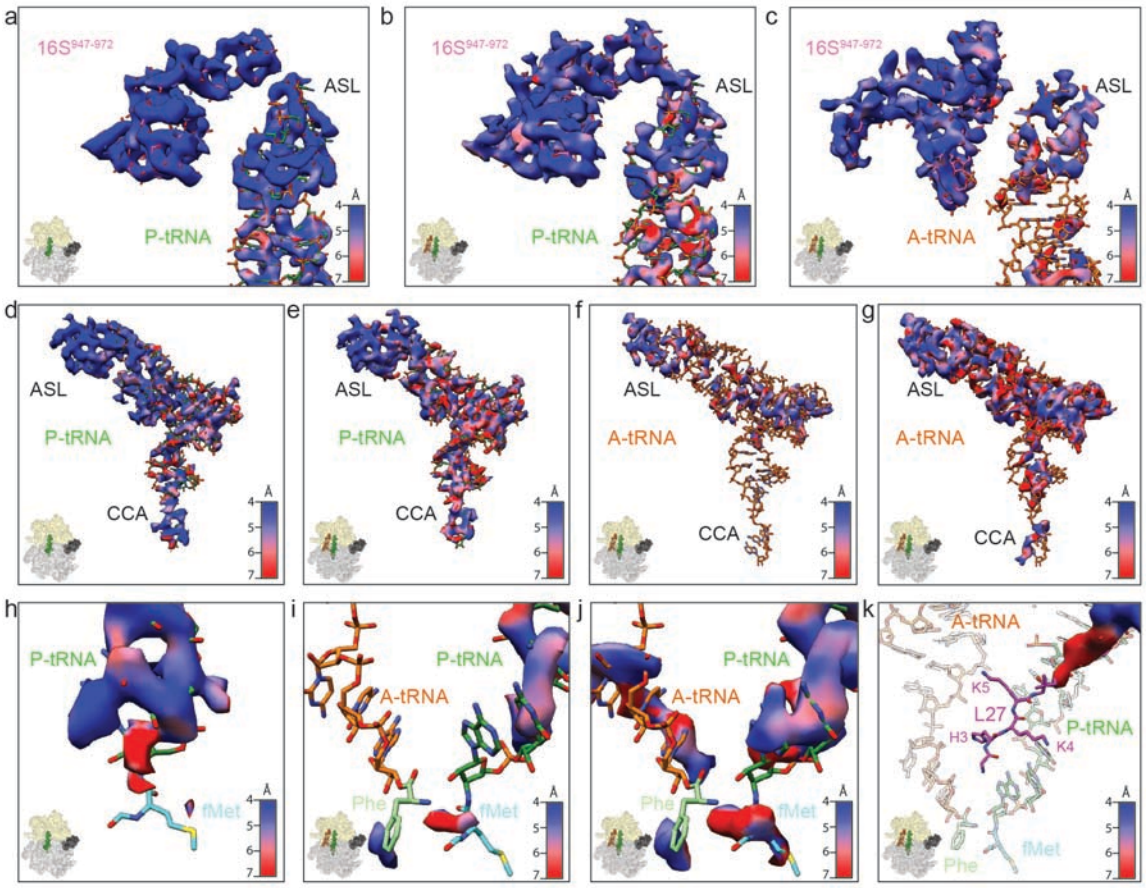

Figure S2 Flexibility of tRNA^{Pro} in A- and P-sites in the absence of EF-P. (**a-c**) Cryo-EM densities coloured according to local resolution of the ASL of P-site tRNA^{Pro} (green) or A-site tRNA^{Pro} (orange) in comparison to nucleotides 947-972 (purple) of the 16S rRNA at high threshold (7σ). (**d-g**) Cryo-EM densities of (**d,e**) P-site tRNA^{Pro} (green) and (**f,g**) tRNA^{Pro} (orange) coloured according to local resolution at (**d-f**) high (7σ) or (**g**) low threshold (3.5σ). (**h-j**) Cryo-EM densities of the CCA-ends of (**h**) P-site tRNA or (**i,j**) P- and A-site tRNAs including modeled fMet (cyan) and Phe (green) (from PDB ID 1V4Y)[29], coloured according to local resolution. (**k**) Cryo-EM density colored according to local resolution for the N-terminus of ribosomal protein L27 (purple).

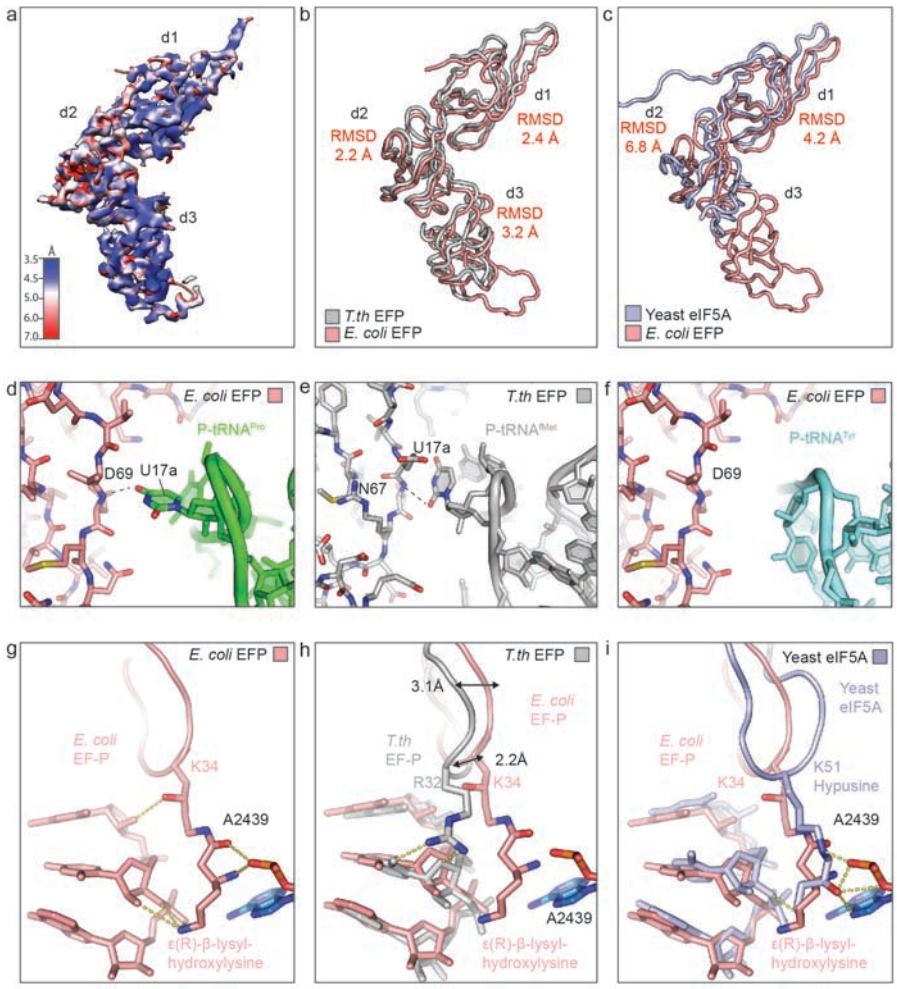

Figure S3 Comparison of *E. coli* EF-P, *T. thermophilus* EF-P and yeast eIF5A on the ribosome. (**a**) Cryo-EM density for EF-P coloured according to local resolution, with EF-P domains labeled (d1-d3). (**b,c**) Superimposition of ribosome-bound conformations of *E. coli* EF-P (salmon) with (**b**) *T. thermophilus* EF-P (grey) (PDB ID 3HUX)[22] and (**c**) yeast eIF5A (light blue) (PDB ID 5GAK)[24]. Root mean square deviations (RMSD) for the individual domains are indicated. (**d**) Interaction of D69 of *E. coli* EF-P with nucleotide U17a of the D-loop of P-site $tRNA^{Pro}$ (green). (**e**) Interaction of N67 of *T. thermophilus* with nucleotide U17a of the D-loop of P-site $tRNA^{fMet}$ (grey)(PDB ID 3HUX)[22]. (**f**) Absence of interaction of D69 of *E. coli* EF-P with the D-loop of a $tRNA^{Tyr}$ (cyan, PDB ID 4WQ1) modeled into the P-site of the ribosome. (**g-i**) Interaction of (**g**) *E. coli* EF-P, (**h**) *T. thermophilus* EF-P (grey)(PDB ID 3HUX)[22] and (**i**) yeast eIF5A (light blue) (PDB ID 5GAK)[24], with the CCA-end of P-site tRNA as well as A2439 (blue) of 23S rRNA (A2808 of 28S rRNA in yeast).

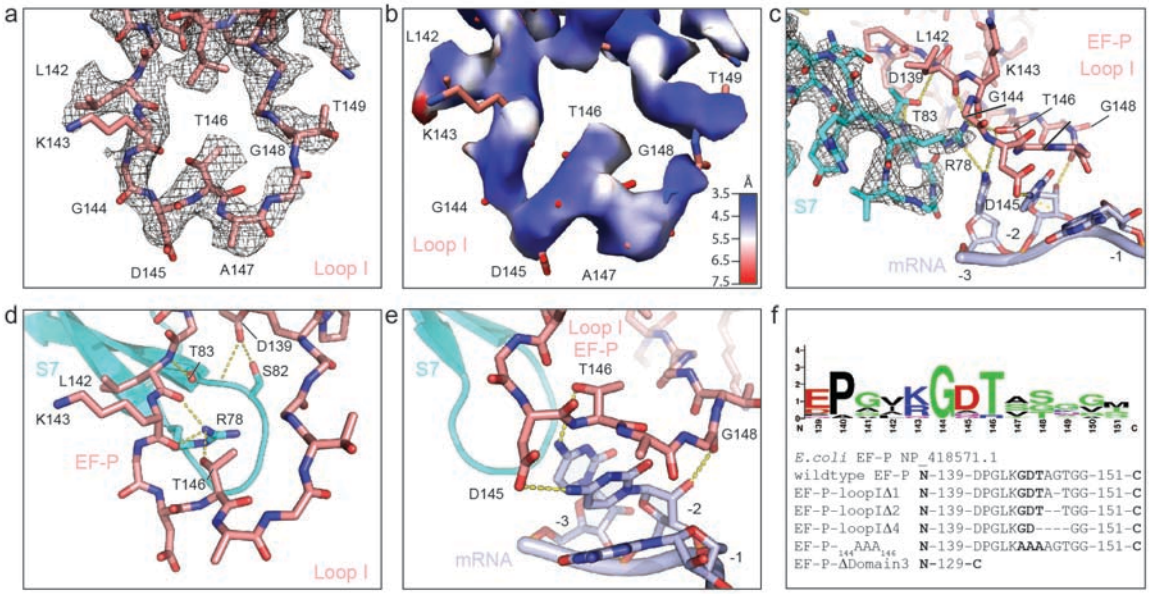

Figure S4 Interactions of Loop I of domain 3 with S7 and the E-site codon. (**a**) Electron density (grey mesh) for loop I of domain 3 (salmon). (**b**) Same as (**a**) but coloured according to local resolution. (**c**) Potential hydrogen bonds between loop I of EF-P (salmon), S7 (cyan) and the E-site codon (light blue) are indicated as dashed lines. (**d**) as (**c**) but only focusing on interactions between S7 and loop I of EF-P. (**e**) as (**c**) but only focusing on the interactions between the E-site codon and loop I. In (**c**) and (**e**), -1, -2 and -3 nucleotides of the E-site codon are relative to the first position of the P-site codon. (**f**) Weblogo of residues of EF-P loop I (based on 12 different bacterial EF-P sequences) and mutation scheme for EF-P variants.

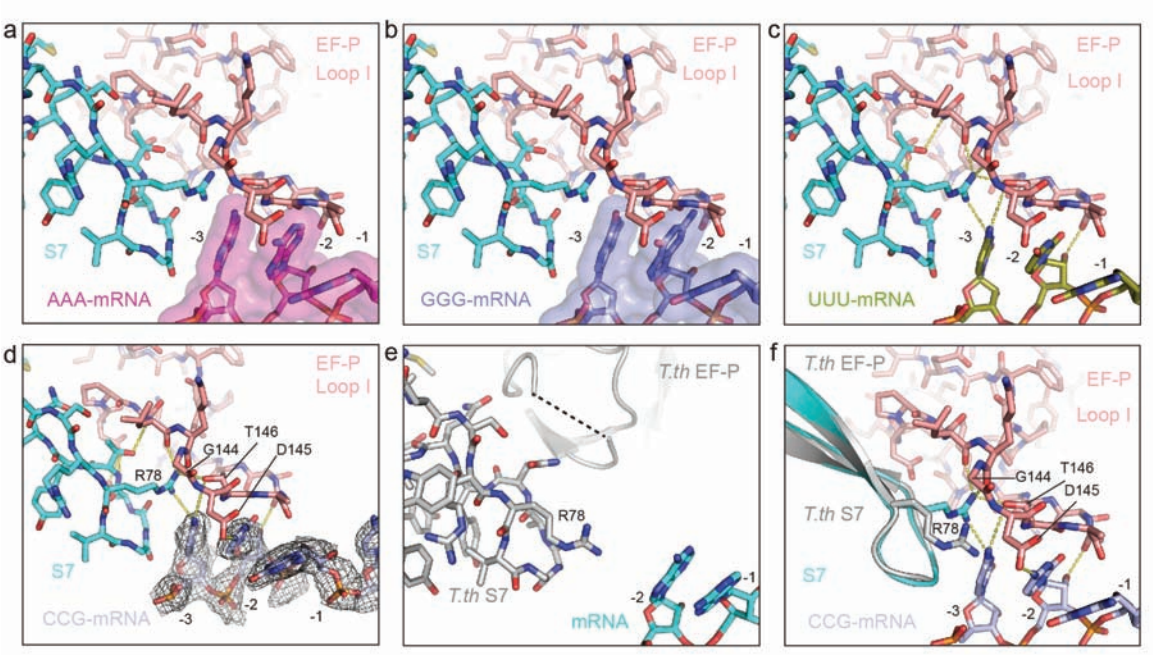

Figure S5 Interaction of Loop I of EF-P with the E-site codon. (**a,b**) Modeling of an (a) AAA (magenta) or (**b**) GGG (blue) codon in the E-site suggests a steric clash with residues within loop I of EF-P (salmon). (**c,d**) Interaction of (**c**) UUU (olive) or (**d**) CCG (light blue) codon in the E-site with loop I of EF-P and S7 (cyan). Potential hydrogen bonds are indicated with dashed yellow lines. Note an additional interaction of loop I of EF-P with the -2 position of the (**d**) proline codon CCG, as compared with (**c**) phenylalanine UUU codon. (**e**) Lack of interaction of *T. thermophilus* (grey) loop I of EF-P with S7 and mRNA (PDB ID 3HUX)[22]. (**f**) Comparison of position of R78 of S7 (grey) from the *T. thermophilus* EF-P (grey) 70S structure (PDB ID 3HUX)[22] or S7 (cyan) from our *E. coli* EF-P-PP-70S structure.

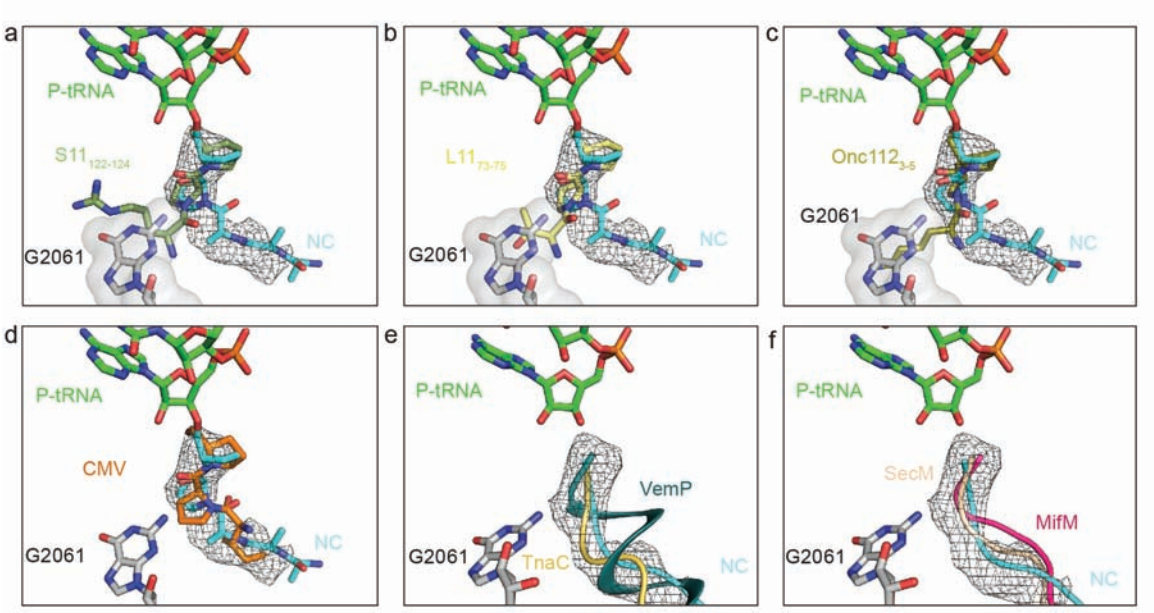

Figure S6 Conformation of polyproline nascent chain on the ribosome. (**a-d**) Comparison of cryo-EM density (mesh) and model for Pro-Pro nascent chain (cyan) compared with conformation of diprolyl residues found in (**a**) S11 (residues 122-124, deep olive), (**b**) L11 (residues 73-75, yellow), (**c**) the antimicrobial peptide Onc112 (residues 3-5, olive, PDB ID 4ZER)[37], and (**d**) the CMV-stalling peptidyl-tRNA (orange, PDB ID 5A8L)[39]. (**e-f**) Comparison of cryo-EM density (mesh) and model for Pro-Pro nascent chain (cyan ribbon) with (e) TnaC (yellow, PDB ID 4UY8)[40], VemP (dark green, PDB ID 5NWY)[41] as well as (f) MifM (pink, PDB ID 3J9W)[42] and SecM (tan, PDB ID 3JBV)[43]. The relative position of nucleotide G2061 (grey) of the 23S rRNA is shown for reference.

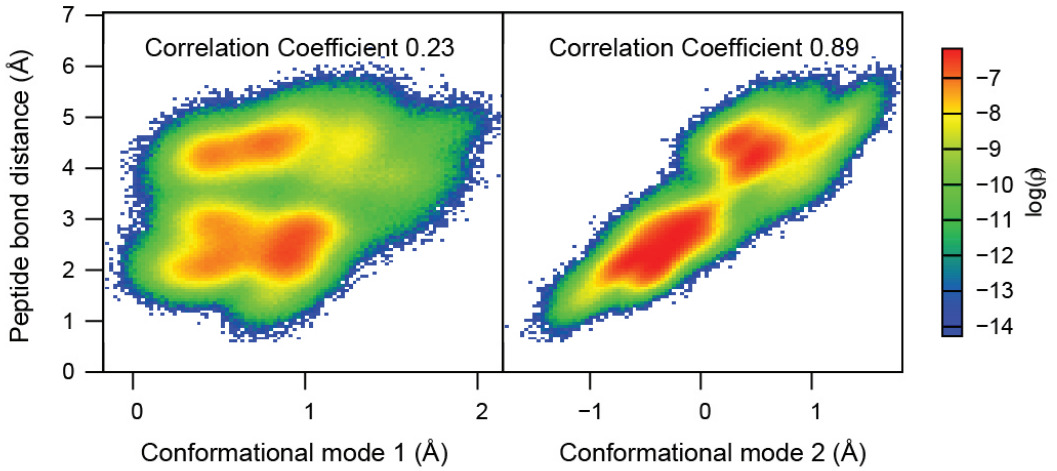

Figure S7 Conformation of polyproline nascent chain on the ribosome. Logarithm of the probability of finding a given peptide bond distance along the first (left panel) or the second (right) conformational mode of the CCA-end and the C-terminal proline backbone atoms obtained from all the simulations. Mode 2 highly correlates (cc=0.89) with the peptide bond distance, while mode 1 describes motions that are largely uncorrelated with the peptide bond distance (cc=0.23).

Supplementary Table 1 Plasmids

Plasmid	Description	Source
pET21b-R_1NlpD	Used for generation of PPP-SRCs	Ref. 25
pET46LIC_*Ec_efp*	Expression of N-terminal His_6-tagged *E.coli* EF-P and its variants (see Table 2)	This study
pRSFDuet_*Ec*_yjeK/*Ec*_yjeA	Co-expression with pET46LIC EF-P	This study

Supplementary Table 2 Primers

Primers for Mutation of pET46LIC_*Ec_efp*	**Sequence**
For EF-P-R186A	5'-GGTGAATACGTCTCT**GCG**GTGAAGTAATGGATC-3'
Rev EF-P-R186A	5'-GATCCATTACTTCAC**CGC**AGAGACGTATTCACC-3'
For EF-P-Y183A	5'-CCCGCTCTGGTGAA**GCG**GTCTCTCGCGTGAAG-3'
Rev EF-P-Y183A	5'-CTTCACGCGAGAGAC**CGC**TTCACCAGAGCGGG-3'
For EF-P-loopIΔ1	5'-CTGAAAGGTGATACCGCAACTGGCGGCAAACCGGC-3'
Rev EF-P-loopIΔ1	5'-GCCGGTTTGCCGCCAGTTGCGGTATCACCTTTCAG-3'
For EF-P-loopIΔ2	5'-GGCCTGAAAGGTGATACCACTGGCGGCAAACCGGC-3'
Rev EF-P-loopIΔ2	5'-GCCGGTTTGCCGCCAGTGGTATCACCTTTCAGGCC-3'
For EF-P-loopIΔ3	5'-CCGGGCCTGAAAGGTGATGGCGGCAAACCGGCTACC-3'
Rev EF-P-loopIΔ3	5'-GGTAGCCGGTTTGCCGCCATCACCTTTCAGGCCCGG-3'
For EF-P-$_{144}$AAA$_{146}$	5'-GATCCGGGCCTGAAA**GCGGCGGCG**GCAGGTACTGGCGGC-3'
Rev EF-P-$_{144}$AAA$_{146}$	5'-GCCGCCAGTACCTGC**CGCCGCCGC**TTTCAGGCCCGGATC-3'
For EF-P-K34A	5'-CGTAAAACCGGGT**GCG**GGCCAGGCATTTG-3'
Rev EF-P-K34A	5'-CAAATGCCTGGCC**CGC**ACCCGGTTTTACG-3'
For EF-P-ΔDomain3	5'-GTTACTCCGCCGAAC**TAA**GTTGAACTGGAAATC-3'
Rev EF-P-ΔDomain3	5'-GATTTCCAGTTCAAC**TTA**GTTCGGCGGAGTAAC-3'